High-Valent Transition Metal Chemistry. Mössbauer and EPR Studies of High-Spin (S = 2) Iron(IV) and Intermediate-Spin (S = $^3/_2$) Iron(III) Complexes with a Macrocyclic Tetraamido-N Ligand

Kimberly L. Kostka,[†] Brian G. Fox,[†] Michael P. Hendrich,[‡] Terrence J. Collins,*[,†] Clifton E. F. Rickard,[§] L. James Wright,[§] and Eckard Münck*[,†]

Contribution from the Departments of Chemistry, Carnegie Mellon University, 4400 Fifth Avenue, Pittsburgh, Pennsylvania 15213, University of Minnesota, Minneapolis, Minnesota 55455, and University of Auckland, Private Bag 92019, Auckland 1, New Zealand

Received January 4, 1993

Abstract: Synthetic iron(IV) complexes are attracting interest both as models for putative intermediates of biochemical reactions as well as for proposed catalytic entities. We have previously reported the X-ray structure of $[Et_4N][Fe^{IV}Cl(\eta^4\text{-MAC*})]$ (H_4[MAC*] = 1,4,8,11-tetraaza-13,13-diethyl-2,2,5,5,7,7,10,10-octamethyl-3,6,9,12,14-pentaoxocyclotetradecane), where iron is coordinated to a plane of four amide nitrogen anions of a macrocyclic ligand and to one axial chloride (Collins, T. J.; Kostka, K. L.; Münck, E.; Uffelman, E. *J. Am. Chem. Soc.* **1990**, *112*, 5637–5639). In zero magnetic field, the 4.2 K Mössbauer spectrum of $[Et_4N][Fe^{IV}Cl(\eta^4\text{-MAC*})]$ was a single quadrupole doublet with ΔE_Q = 0.89 mm/s and δ = –0.02 mm/s, consistent with an iron(IV) assignment. Here we present full synthetic and characterization results together with detailed Mössbauer and integer spin EPR studies of $[Fe^{IV}Cl(\eta^4\text{-MAC*})]^-$ prepared with $[Ph_4P]^+$, $[Et_4N]^+$, $[n\text{-}Bu_4N]^+$, and $[PPN]^+$ counterions. In strong applied fields, the Mössbauer spectra exhibit magnetic hyperfine patterns typical of complexes with integer electronic spin. The zero-field splitting parameters (D = –2.6 cm^{-1} and E/D = 0.13) are such that the two lowest spin levels of the ground multiplet are nearly degenerate (Δ = 0.16 cm^{-1}). Correspondingly, $[Fe^{IV}Cl(\eta^4\text{-MAC*})]^-$ exhibits an integer spin EPR resonance at X-band with g_{eff} = 8.0, indicative of a high-spin (S = 2) ground configuration. Quantitative analysis of the integer spin EPR spectra observed from both frozen CH_3CN solution and from polycrystalline samples shows that the principal g-values are less than 2, as expected for high-spin iron(IV), and that the spin concentration of the S = 2 species agrees within 12% with the concentration determined by optical spectroscopy. We also report synthetic details and the X-ray structure of $[Et_4N]_2[Fe^{III}Cl(\eta^4\text{-MAC*})]\cdot CH_2Cl_2\cdot H_2O$. Crystals of $[Et_4N]_2[Fe^{III}Cl(\eta^4\text{-MAC*})]\cdot CH_2Cl_2\cdot H_2O$ at 293 K are monoclinic, space group $P2_1/n$, with a = 11.797(9) Å, b = 18.662(6) Å, c = 21.984(8) Å, β = 102.75(6)°, V = 4708.6 Å^3, Z = 4 (d_{calcd} = 1.423 g cm^{-3}), μ_α(Mo Kα) = 3.92 cm^{-1}, and R_1 (unweighted, based on F) = 0.086 for 3298 observed reflections [$I > 3\sigma(I)$]. Mössbauer and EPR studies show that this complex has an intermediate-spin (S = $^3/_2$) ground state with hyperfine parameters similar to those reported for the porphyrin complex $[Fe^{III}(TPP)(FSbF_5)]$ (Gupta, G. P.; Lang, G.; Reed, C. A.; Shelly, K.; Scheidt, W. R. *J. Chem. Phys.* **1987**, *86*, 5288–5293). However, the zero-field splitting tensor of $[Et_4N]_2[Fe^{III}Cl(\eta^4\text{-MAC*})]$ (D = –3.7 cm^{-1}, E/D = 0.05) is rotated by 90° relative to the magnetic hyperfine and electric field gradient tensors. Analysis of the high-field Mössbauer spectra for both $[Fe^{III}Cl(\eta^4\text{-MAC*})]^{2-}$ and $[Fe^{IV}Cl(\eta^4\text{-MAC*})]^-$ reveals magnetic hyperfine interactions substantially smaller than expected for an ionic complex, suggesting substantial covalency for both redox states.

Our research groups have longstanding interests in the study of high-valent iron species. In part, this interest arises because iron(IV) intermediates have been shown to exist for the heme peroxidases[1] and have been postulated for cytochrome P-450[2] and proteins such as methane monooxygenase,[3] ribonucleotide reductase,[4] isopenicillin N-synthase,[5] phenylalanine hydroxylase,[6] and others.[7] An iron(IV) intermediate obtained from the synthetic hydrocarbon oxidation catalyst $Fe_2TPA_2O(ClO_4)_4$ has been recently characterized by spectroscopic methods,[8] while high-valent iron species have been proposed on the basis of catalytic studies for a variety of other oxidation systems.[9] The under-

* Authors to whom correspondence should be directed.
† Carnegie Mellon University.
‡ University of Minnesota.
§ University of Auckland.

(1) (a) Schulz, C. E.; Rutter, R.; Sage, J. T.; Debrunner, P. G.; Hager, L. P. *Biochemistry* **1984**, *23*, 4743–4754. (b) Rutter, R.; Hager, L. P.; Dhonau, H.; Hendrich, M. P.; Valentine, M.; Debrunner, P. G. *Biochemistry* **1984**, *23*, 6809–6816. (c) Rutter, R.; Valentine, M.; Hendrich, M. P.; Hager, L. P.; Debrunner, P. G. *Biochemistry* **1983**, *22*, 4769–4774. (d) LaMar, G. N.; de Ropp, J. S.; Latos-Grazynski, L.; Balch, A. L.; Johnson, R. B.; Smith, K. M.; Parish, D. W.; Cheng, R.-J. *J. Am. Chem. Soc.* **1983**, *105*, 782–787. (e) Roberts, J. E.; Hoffman, B. M.; Rutter, R.; Hager, L. M. *J. Biol. Chem.* **1981**, *256*, 2118–2121.

(2) (a) Groves, J. T.; Watanabe, Y. *J. Am. Chem. Soc.* **1988**, *110*, 8443–8452. (b) McMurray, T. J.; Groves, J. T. In *Cytochrome P-450: Structure, Mechanism, and Biochemistry*; Ortiz de Montellano, P. R., Ed.; Plenum Press: New York, 1986; pp 1–28.

(3) (a) Fox, B. G.; Borneman, J. G.; Wackett, L. P.; Lipscomb, J. D. *Biochemistry* **1990**, *29*, 6419–6427. (b) Fox, B. G.; Froland, W. A.; Dege, J. E.; Lipscomb, J. D. *J. Biol. Chem.* **1989**, *264*, 10023–10033.

(4) (a) Elgren, T. E.; Lynch, J. B.; Juarez-Garcia, C.; Münck, E.; Sjöberg, B.-M.; Que, L., Jr. *J. Biol. Chem.* **1991**, *266*, 19265–19268. (b) Sanders-Loehr, J. *Prog. Clin. Biol. Res.* **1988**, *274*, 193–209.

(5) Baldwin, J. E.; Abraham, E. P. *Nat. Prod. Rep.* **1988**, *5*, 129–145.

(6) Dix, T. A.; Benkovic, S. J. *Acc. Chem. Res.* **1988**, *21*, 101–107.

(7) (a) Buist, P. H.; Marecak, D. M. *J. Am. Chem. Soc.* **1992**, *114*, 5073–5080. (b) Fu, H.; Newcomb, M.; Wong, C.-H. *J. Am. Chem. Soc.* **1991**, *113*, 5878–5880. (c) Colbert, J. E.; Katopodis, A. G.; May, S. W. *J. Am. Chem. Soc.* **1990**, *112*, 3993–3996.

(8) Leising, R. L.; Brennan, B. A.; Que, L., Jr.; Fox, B. G.; Münck, E. *J. Am. Chem. Soc.* **1991**, *113*, 3988–3990.

(9) (a) Barton, D. H. R.; Doller, D. *Acc. Chem. Res.* **1992**, *25*, 504–512. (b) Tung, H.-C.; Kang, C.; Sawyer, D. T. *J. Am. Chem. Soc.* **1992**, *114*, 3445–3455. (c) Stassinopoulos, A.; Schulte, G.; Papaefthymiou, G. C.; Caradonna, J. P. *J. Am. Chem. Soc.* **1991**, *113*, 8686–8697. (d) Natrajan, A.; Hecht, S. M.; van der Marel, G. A.; van Boom, J. H. *J. Am. Chem. Soc.* **1990**, *112*, 3997–4002. (e) Balasubrumanian, P. N.; Bruice, T. C. *J. Am. Chem. Soc.* **1986**, *108*, 5495–5503.

0002-7863/93/1515-6746$04.00/0

Scheme I

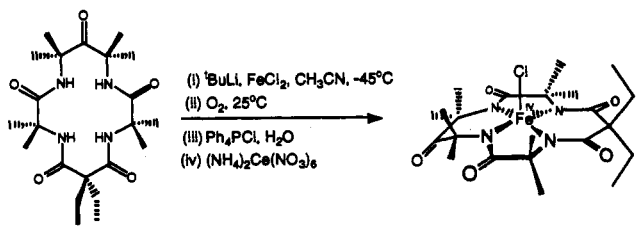

H_4[MAC*] Ph_4P[Fe(IV)Cl(η^4-MAC*)]

standing of the structural, electronic, and catalytic properties of these reactive intermediates could be greatly enhanced by the detailed characterization of stable iron(IV) coordination complexes using spectroscopic techniques. We are also interested in iron(IV) chemistry because the diversity of the above mentioned biological and synthetic systems strongly suggests that a large nonbiological chemistry of iron(IV) should be accessible, yet this area remains comparatively unexplored and presents a significant challenge for synthetic inorganic chemists.

During the past few years, we have developed a strategy for the synthesis of highly donating, oxidant-resistant tetraamido-*N* macrocycles that allow stabilization of high oxidation state complexes of a variety of transition metals, including strongly oxidizing species.[10] Using one of these macrocycles, we have recently provided a preliminary communication describing the synthesis and the molecular and structural properties of $[Et_4N][FeCl(\eta^4\text{-MAC*})]$ (see Scheme I).[10d,11] On the basis of the observed Mössbauer isomer shift, we concluded that this five-coordinate complex was at the iron(IV) oxidation state. Our present results confirm that this iron(IV) anionic complex is stable as a number of salts of varying solubility and that the macrocyclic ligand is electrochemically inert over a wide potential range. This behavior has allowed for the detailed exploration of the electronic structure of the $[FeCl(\eta^4\text{-MAC*})]^-$ anion presented here.

The present studies demonstrate that the $[FeCl(\eta^4\text{-MAC*})]^-$ anion is, to the best of our knowledge, the first homogeneous coordination compound to exhibit a high-spin ($S = 2$) iron(IV) configuration. The high-spin configuration has been previously observed in synthetic ferrites with the perovskite structure, $M_{0.5}La_{1.5}Li_{0.5}Fe_{0.5}O_4$ (where M = Ca, Sr, or Ba).[12] In these solids, a pronounced tetragonal elongation of the FeO_6 octahedron is associated with the stabilization of the high-spin $^5A_1$ manifold. The extended lattice of the perovskites exhibits magnetic ordering at low temperatures. In contrast, $[FeCl(\eta^4\text{-MAC*})]^-$ is paramagnetic both as a solid and in frozen solution, allowing the magnetic hyperfine tensor, the electric field gradient (EFG) tensor, and the zero field splitting (ZFS) tensor to be determined by Mössbauer spectroscopy. Moreover, the values of the ZFS parameters allow the relatively new technique of integer spin EPR to be utilized in the characterization of this iron(IV) complex.[13]

For analogues with the same ligand complement, but with different spin and/or oxidation states, it is also useful to be able to make comparisons of the spectroscopic data. Accordingly, the compound $[Et_4N]_2[Fe^{III}Cl(\eta^4\text{-MAC*})]\cdot CH_2Cl_2$, the immediate synthetic precursor to $[Et_4N][Fe^{IV}Cl(\eta^4\text{-MAC*})]$, has also been characterized by X-ray crystallography, elemental analysis, cyclic voltammetry, and IR, UV/vis, X-band EPR, and Mössbauer spectroscopies to allow for this comparison. Interestingly, $[Et_4N]_2[Fe^{III}Cl(\eta^4\text{-MAC*})]\cdot CH_2Cl_2$ has been found to belong to a small group of iron(III) complexes with an intermediate-spin $S = {}^3/_2$ ground state. Although the intermediate-spin $S = {}^3/_2$ state has been studied extensively for hemes and dithiocarbamates,[14] the electronic structure of this spin state is still poorly understood. The Mössbauer and EPR studies of the $S = {}^3/_2$ ground manifold of $[Et_4N]_2[Fe^{III}Cl(\eta^4\text{-MAC*})]\cdot CH_2Cl_2$ reported here provide a complete set of spin Hamiltonian parameters obtained from extensive spectral simulations. These and comparable studies of $[Et_4N][Fe^{IV}Cl(\eta^4\text{-MAC*})]$ reveal that both redox states of $[FeCl(\eta^4\text{-MAC*})]^{n-}$ exhibit substantial covalency.

Experimental Section

Materials and Reagents. All solvents and reagents were Fisher reagent grade unless otherwise indicated, and all materials were used as received. Microanalyses were performed by Midwest Microlabs, Indianapolis, IN, and by The Chemical Analysis Laboratory, Institute of Ecology, University of Georgia, Athens, GA. Iron was also determined colorimetrically.[15]

Syntheses. $Li_2[Fe^{III}Cl(\eta^4\text{-MAC*})]$. H_4[MAC*][10b] (742 mg, 1.42 mmol) was dissolved in CH_3CN (40 mL, Aldrich) under N_2. *tert*-Butyllithium (4.0 mL, 6.8 mmol, 1.7 M in 2,4-dimethylpentane, Aldrich) was added under N_2 to the solution at −45 °C. Ferrous chloride (anhydrous, 260 mg, 2.05 mmol, Alfa) was added to the mixture under N_2. The solution was allowed to warm to room temperature and was stirred (2 h), yielding an olive-green precipitate. Air was admitted through a drying tube (2 h), and the solid was collected and washed with CH_2Cl_2 (2 × 10 mL) and hexanes (10 mL). The resulting orange powder was dried under reduced pressure. Yield: 912 mg (~99%). Because of variable solvation and limited solubility, this material was converted to a nonlithium salt for further characterization. IR (Nujol): 1711 cm^{-1} (ν(CO)ketone), 1609 cm^{-1} (ν(CO)amide), 1575 cm^{-1} (ν(CO)amide), 1552 cm^{-1} (ν(CO)amide).

$[Et_4N]_2[Fe^{III}Cl(\eta^4\text{-MAC*})]\cdot CH_2Cl_2$. $Li_2[Fe^{III}Cl(\eta^4\text{-MAC*})]$ (340 mg, ~0.63 mmol) was stirred in CH_2Cl_2 with $[Et_4N]Cl\cdot xH_2O$ (1.34 g, Aldrich) overnight. Bright orange-red crystals were grown from CH_2Cl_2/hexane at 4 °C by repeatedly separating excess salt, which crystallized as a white salt from the mother liquor, until only orange crystals formed. Yield: 245 mg, ~45%. Anal. Calcd for $C_{39}H_{76}N_6O_5Cl_3Fe$: C, 53.76; H, 8.79; N, 9.65; Cl, 12.21. Found: C, 53.69; H, 8.86; N, 9.69; Cl, 12.17. The molar absorptivity was determined in CH_3CN (Figure 4) on five separately weighed samples (mass range: 25–50 mg) from one preparation. A propagation of errors analysis was performed on the resulting data. Within the 3σ confidence level, the molar absorptivity obtained was ϵ_{440} = 7600 ± 400 L mol^{-1} cm^{-1}.

$[Ph_4P][Fe^{IV}Cl(\eta^4\text{-MAC*})]\cdot C_6H_6$. $Li_2[Fe^{III}Cl(\eta^4\text{-MAC*})]$ (290 mg, ~0.54 mmol) was stirred in deionized water (15 mL, 20 min), and the resulting red-orange solution was centrifuged and filtered to remove residual solids. $[Ph_4P][Cl]$ (609 mg, 1.6 mmol, Aldrich) was dissolved in the orange solution by stirring (10 min), and $[NH_4]_2[Ce(NO_3)_6]$ (607 mg, 1.1 mmol, Aldrich) was added while the reaction solution was stirred vigorously. The black precipitate of $[Ph_4N][Fe^{IV}Cl(\eta^4\text{-MAC*})]$ which formed rapidly was collected and washed with deionized water (2 × 20 mL). The fine black powder (287 mg) was dried in a vacuum desiccator (1.5 h) and then dissolved in benzene/CH_2Cl_2 (170 mL/60 mL). This

(10) (a) Collins, T. J.; Fox, B. G.; Hu, Z. G.; Kostka, K. L.; Münck, E.; Rickard, C. E. F.; Wright, L. J. *J. Am. Chem. Soc.* **1992**, *114*, 8724–8725. (b) Collins, T. J.; Kostka, K. L.; Uffelman, E. S.; Weinberger, T. L. *Inorg. Chem.* **1991**, *30*, 4204–4210. (c) Collins, T. J.; Slebodnick, C.; Uffelman, E. S. *Inorg. Chem.* **1990**, *29*, 3433–3436. (d) Collins, T. J.; Kostka, K. L.; Münck, E.; Uffelman, E. S. *J. Am. Chem. Soc.* **1990**, *112*, 5737–5639.

(11) The parent macrocyclic tetraprotonated ligand is systematically named as 1,4,8,11-tetraaza-13,13-diethyl-2,2,5,5,7,7,10,10-octamethyl-3,6,9,12,14-pentaoxocyclotetradecane. For the purposes of clarity in the discussion section, we will introduce the abbreviated symbol, $[\eta^4\text{-MAC*}]^{4-}$, for the coordinated tetraanionic macrocyclic ligand. The H_4[MAC*] symbol has been chosen because the macrocyclic ligand is alkylated at every ring position where a C–H bond would be found in the simplest homologue. The symbol mimics the useage of Cp^{*-} for the permethylated cyclopentadienyl anion.

(12) (a) Demazeau, G.; Chevreau, N.; Fournes, L.; Soubeyroux, J.-L.; Takeda, Y.; Thomas, M.; Pouchard, M. *Rev. de Chim. Miner.* **1983**, *20*, 155–172. (b) Demazeau, G.; Li-Ming, Z.; Fournes, L.; Pouchard, M.; Hagenmuller, P. *J. Solid State Chem.* **1988**, *72*, 31–37.

(13) (a) Münck, E.; Surerus, K. K.; Hendrich, M. P. *Meth. Enzymol.* **1993**, *54*, 346–379. (b) Hendrich, M. P.; Debrunner, P. G. *Biophys. J.* **1989**, *56*, 489–506.

(14) (a) Maltempo, M. M.; Moss, T. H. *Q. Rev. Biophys.* **1976**, *9*, 181–215. (b) Gupta, G. P.; Lang, G.; Scheidt, W. R.; Geiger, D. K.; Reed, C. A. *J. Chem. Phys.* **1986**, *85*, 5212–5220. (c) Gupta, G. P.; Lang, G.; Reed, C. A.; Shelly, K.; Scheidt, W. R. *J. Chem. Phys.* **1987**, *86*, 5288–5293. (d) Wickman, H. H.; Trozzolo, A. M. *Inorg. Chem.* **1968**, *7*, 63–68. (e) Chapps, G. E.; McCann, S. W.; Wickman, H. H.; Sherwood, R. C. *J. Chem. Phys.* **1974**, *60*, 990–997. (f) Wickman, H. H.; Trozzolo, A. M.; Williams, H. J.; Gull, G. W.; Merritt, F. R. *Phys. Rev.* **1967**, *155*, 563–566.

(15) Brumby, P. E.; Massey, V. *Meth. Enzymol.* **1967**, *10*, 463–474.

solution was dried over $MgSO_4$ (10 min), and the solvent was removed under reduced pressure (120 mL). Black crystals were grown by vapor diffusion of hexane into the benzene solution at 4 °C and separated manually from the orange oil of the iron(III) salt which forms slowly on standing in solution. The crystals were washed sparingly in deionized water (2 × 5 mL). Yield: 129 mg, 25%. Anal. Calcd for $C_{52}H_{60}N_4O_5ClFeP$: C, 66.21; H, 6.41; N, 5.94; Cl, 3.76; P, 3.28. Found: C, 66.12; H, 6.37; N, 5.99; Cl, 3.80; P, 3.25. Molar absorptivities were determined in CH_3CN (Figure 4) on five separately weighed samples (mass range: 20–42 mg) from one preparation for which there was a corresponding satisfactory elemental analysis to confirm purity. Due to the slow conversion of the iron(IV) to the iron(III) species in CH_3CN, the solutions were measured in a sealed cuvette within 5 min of their preparation. (The iron(IV) to iron(III) conversion is not found in CH_2Cl_2, but this solvent was avoided for Mössbauer studies due to the strong absorption of the 14-keV γ-rays.) A propagation of errors analysis was performed on the resulting data, and the standard error (67 L mol^{-1} cm^{-1}) was found to lie within the 1σ confidence level. Within the 3σ confidence level, the molar absorptivities obtained were as follows: ϵ_{450} = 10 900 ± 500 L mol^{-1} cm^{-1}; ϵ_{672} = 4100 ± 480 L mol^{-1} cm^{-1}.

$[Bu_4N][Fe^{IV}Cl(\eta^4\text{-MAC*})]$. $[Et_4N]_2[Fe^{III}Cl(\eta^4\text{-MAC*})]$ (84 mg, 96 mmol in 100 mL CH_2Cl_2, Aldrich Sureseal, with 0.05 M $[Bu_4N][ClO_4]$, Fluka) was electrochemically oxidized at a potential of +780 mV vs a Ag wire quasi-reference electrode until current flow ceased, producing a black solution. The solvent was removed under reduced pressure. The resulting black solid was dissolved in benzene and was recovered by fractional crystallization from benzene/cyclohexane at 4 °C. During the first few days of the crystallization process, the mother liquor was decanted from the colorless crystals of $[Bu_4N][ClO_4]$ until these ceased to form, at which time black crystals of $[Bu_4N][Fe^{IV}Cl(\eta^4\text{-MAC*})]$ began to form. After 1 week, shiny black crystals were collected and separated manually from small quantities of an orange oil consisting of the iron(III) salt. Yield: 40 mg, 64%.

$[Et_4N][Fe^{IV}Cl(\eta^4\text{-MAC*})]$. $[Et_4N]_2[Fe^{III}Cl(\eta^4\text{-MAC*})]$ (103 mg, 0.118 mmol in 100 mL CH_2Cl_2, Aldrich Sureseal) was electrochemically oxidized at a potential of +780 mV vs a Ag wire quasi-reference electrode with $[Et_4N][ClO_4]$ (1.079 g, 47 mM, Fluka) as supporting electrolyte until current flow ceased. During the course of the oxidation, the orange solution became black. Upon completion of the oxidation, the solvent was removed under reduced pressure and the resulting black solid was dissolved in benzene/CH_2Cl_2 (250 mL/50 mL). The CH_2Cl_2 was removed under reduced pressure, causing $[Et_4N][ClO_4]$ to precipitate from solution. After excess salt was removed, shiny black crystals were grown from benzene/hexane at 4 °C and were separated manually from small amounts of an orange oil consisting of the iron(III) salt. Yield: 42 mg, 64 μmol, 54%. IR (Nujol): 1712 cm^{-1} (ν(CO)ketone), 1618 cm^{-1} (ν(CO)amide), 1599 cm^{-1} (ν(CO)amide), 1577 cm^{-1} (ν(CO)amide).

^{57}Fe-Enriched $^{57}FeCl_2$. ^{57}Fe metal foil (95% isotopic enrichment, 13 mg, Atomergic Chemetals, Farmington, NY) was added to a three-necked flask containing Fe metal powder (98 mg, Aldrich) to give a final isotopic enrichment of 12%. Concentrated HCl (4.0 mL) and methanol (7.0 mL) were added, and the mixture was stirred under N_2 until all metal was dissolved (48 h). The solvent was then removed under reduced pressure. The remaining powder was heated to 170 °C and dried under vacuum (3 h). For preparation of ^{57}Fe-enriched $Li_2[Fe^{III}Cl(\eta^4\text{-MAC*})]$, metal was inserted by adding the ligand, solvent, and base directly to the three-necked flask containing the freshly prepared ^{57}Fe-enriched $FeCl_2$.

$[PPN][^{(12\%)57}Fe^{IV}Cl(\eta^4\text{-MAC*})]$. $Li_2[^{(12\%)57}Fe^{III}Cl(\eta^4\text{-MAC*})]$ (239 mg, ca. 0.44 mmol) was stirred in deionized water (20 mL, 20 min), and the resulting red-orange solution was centrifuged (40 min), decanted, and filtered to remove insoluble iron residues. Bis(triphenylphosphoranylidene)ammonium chloride ([PPN][Cl], 779 mg, 1.36 mmol, Aldrich), MeOH (0.5 mL), and CH_3CN (1 mL) were added to the solution. This mixture was vigorously stirred, and then $[NH_4]_2[Ce(NO_3)_6]$ (1.13 g, 2.1 mmol, Aldrich) was added with continued stirring. The resulting black precipitate, $[PPN][Fe^{IV}Cl(\eta^4\text{-MAC*})]$, was collected and washed with deionized water (3 × 10 mL). The fine black powder was dried in a vacuum desiccator (2 h) and was then dissolved in benzene (75 mL). The solvent volume was reduced (45 mL), and crystals were grown by vapor diffusion of cyclohexane into the benzene solution. Yield: 119 mg, 0.12 mmol, ca. 25%. Anal. Calcd for $C_{58}H_{64}N_5O_5Cl^{(12\%)57}FeP_2$: C, 65.44; H, 6.06; N, 6.58. Found: C, 65.28; H, 5.97; N, 6.34.

X-ray Crystal Structure Data and Refinement for $[Et_4N]_2[Fe^{III}Cl(\eta^4\text{-MAC*})]\cdot CH_2Cl_2\cdot H_2O$. Cell and data collection parameters are given in Table I, and the structure of $[Fe^{III}Cl(MAC*)]^{2-}$ present in the crystal is shown in Figure 1. Single crystals of $[Et_4N]_2[Fe^{III}Cl(\eta^4\text{-MAC*})]\cdot CH_2Cl_2\cdot H_2O$ were sealed in thin-walled glass capillaries. Cell parameters were obtained by least-squares fit to the setting angles of 25 reflections. Three reflections monitored throughout data collection showed a steady decline in intensity to 62% of the original value. The data were corrected for Lorentz, polarization, and decomposition. Absorption corrections were applied using an empirical φ curve.[16] The structure was solved by direct methods,[17] and all atoms of the anion and one from the cation were identified in the initial E map. The remaining atoms were identified in subsequent electron density maps. The structure was refined by a full-matrix least-squares treatment.[18] While the anion and one cation refined well, the second cation and the dichloromethane solvate showed evidence of disorder. In the case of the chlorine atoms of the dichloromethane, the anisotropic thermal parameter was allowed to take up the disorder. For the tetraethylammonium group, one terminal carbon atom resolved into two peaks and was treated as two half-weighted atoms. The remaining atoms could not be resolved, and the thermal parameter has been allowed to cover the disorder. For the well-refined anion and cation, hydrogen atoms were included in calculated positions and were allowed to ride on

Table I. Experimental Data for Structural Determination of $[Et_4N]_2[Fe(III)(Cl)(\eta^4\text{-MAC*})]\cdot CH_2Cl_2\cdot H_2O$

formula	$C_{39}H_{78}Cl_3FeN_6O_6$
fw	889.31
cryst system	monoclinic
space group	$P2_1/n$
unit cell constraints	a = 11.767(9), b = 18.662(6), c = 21.984(8) Å; β = 102.75(6)°; C = 4708.6 Å^3
D_{calcd} (Z = 4)	1.423 g cm^{-3}
F(000)	2156
μ	3.92 cm^{-1}
Mo Kα (monochromatic) λ	0.710 69 Å
temp	293 K
diffractometer	Nonius CAD4
scan technique	$\omega/2\theta$
2θ(min–max)	2–50°
no. of unique reflcns	6645
no. of obsd reflcns	3298 [$I > 3\sigma(I)$]
cryst color, size	orange, 0.20 × 0.35 × 0.50 mm
A(min–max)	0.84–1.00
least-squares weights	$1.0/[\sigma(F^2) + 0.0001F^2]$
function minimized	$\sum w[\|F_o\| - \|F_c\|]^2$
R, R'	0.086, 0.091

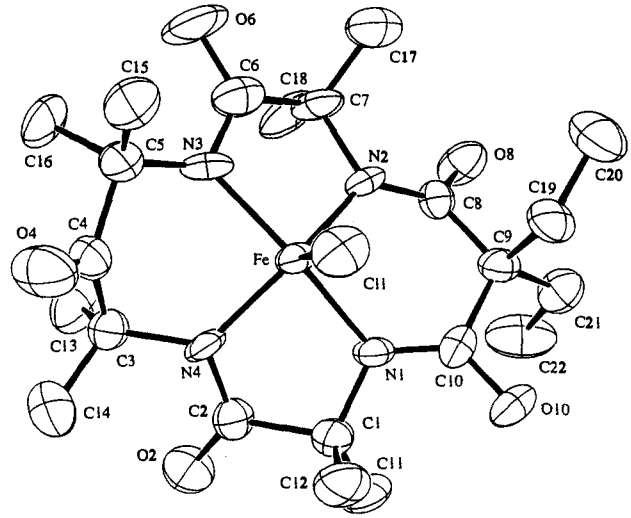

Figure 1. Structure of the $[Fe^{III}Cl(\eta^4\text{-MAC*})]^{2-}$ in the crystal of $[Et_4N]_2[Fe^{III}Cl(\eta^4\text{-MAC*})]\cdot CH_2Cl_2\cdot H_2O$. All non-hydrogen atoms are represented by thermal vibrational ellipsoids drawn to encompass 50% of their electron density; hydrogen atoms are omitted for clarity.

(16) North, A. C.; Phillips, D. C.; Mathews, F. S. *Acta Crystallogr., Sect. A* **1968**, *24*, 315.
(17) Sheldrick, G. M. Institut für Anorganische Chemie, Universität Gottenburg, Germany, 1986.
(18) Sheldrick, G. M. University Chemical Laboratory, Cambridge, England, 1976.

Table II. Selected Bond Lengths and Angles for $(Et_4N)_2[Fe^{III}(Cl)\eta^4\text{-MAC*}]\cdot CH_2Cl_2\cdot H_2O$ with Estimated Standard Deviations in Parentheses

	Interatomic Distances (Å)		
Fe–Cl	2.406(6)	C2–C1	1.54(3)
Fe–N1	1.932(16)	C11–C1	1.52(3)
Fe–N2	1.916(17)	C12–C1	1.53(3)
Fe–N3	1.932(17)	C4–C3	1.51(3)
Fe–N4	1.927(16)	C13–C3	1.50(3)
N1–C1	1.50(3)	C14–C3	1.57(3)
N1–C10	1.29(3)	C5–C4	1.56(3)
N2–C2	1.36(3)	C15–C5	1.52(3)
N2–C3	1.47(3)	C16–C5	1.54(3)
N3–C5	1.46(3)	C7–C6	1.50(3)
N3–C6	1.34(3)	C17–C7	1.51(3)
N4–C7	1.46(2)	C18–C7	1.51(3)
N4–C8	1.33(2)	C9–C8	1.52(3)
C2–O2	1.23(2)	C10–C9	1.52(3)
C4–O4	1.21(3)	C19–C9	1.54(3)
C6–O6	1.28(3)	C21–C9	1.55(3)
C8–O8	1.25(2)	C20–C19	1.53(3)
C10–O10	1.26(2)	C22–C21	1.48(3)
	Bond Angles (deg)		
N1–Fe–Cl	96.7(5)	C14–C3–C4	104.1(19)
N2–Fe–Cl	102.6(5)	C14–C3–C13	108(2)
N2–Fe–N1	83.8(7)	C3–C4–O4	122(2)
N3–Fe–Cl	97.5(5)	C5–C4–O4	118(2)
N3–Fe–N1	165.8(7)	C5–C4–C3	119.9(19)
N3–Fe–N2	92.8(7)	C4–C5–N3	109.4(17)
N4–Fe–Cl	109.5(5)	C15–C5–N3	108.6(18)
N4–Fe–N1	91.6(7)	C15–C5–C4	109(2)
N4–Fe–N2	147.9(7)	C16–C5–N3	116(2)
N4–Fe–N3	83.9(7)	C16–C5–C4	105.2(19)
C1–N1–Fe	113.0(13)	C16–C5–C15	109(2)
C10–N1–Fe	123.4(13)	O6–C6–N3	123(3)
C10–N1–C1	119.0(16)	C7–C6–N3	116.7(19)
C2–N2–Fe	114.5(14)	C7–C6–O6	120(2)
C3–N2–Fe	124.6(13)	C6–C7–N4	107.0(17)
C3–N2–C2	118.0(17)	C17–C7–N4	112.2(19)
C5–N3–Fe	125.4(13)	C17–C7–C6	107.9(19)
C6–N3–Fe	114.0(15)	C18–C7–N4	111.8(17)
C6–N3–C5	118.9(18)	C18–C7–C6	107(2)
C7–N4–Fe	114.9(13)	C18–C7–C17	110(2)
C8–N4–Fe	124.0(12)	O8–C8–N4	122.4(18)
C8–N4–C7	119.6(17)	C9–C8–N4	119.4(17)
C2–C1–N1	104.0(16)	C9–C8–O8	117.6(17)
C11–C1–N1	111.2(19)	C10–C9–C8	116.8(17)
C11–C1–C2	110.3(18)	C19–C9–C8	106.1(16)
C12–C1–N1	113.9(17)	C19–C9–C10	108.0(17)
C12–C1–C2	106(2)	C21–C9–C19	110.0(18)
C12–C1–C11	110.7(19)	C21–C9–C8	109.2(16)
O2–C2–N2	127(2)	C21–C9–C10	106.7(16)
C1–C2–N1	111.4(17)	O10–C10–N1	125(2)
C1–C2–O2	121.1(19)	C9–C10–N1	119.2(17)
C4–C3–N2	106.5(16)	C9–C10–O10	116.1(19)
C13–C3–N2	111.5(19)	C20–C19–C9	115.4(19)
C13–C3–C4	113.1(19)	C22–C21–C9	114(2)
C14–C3–N2	113.0(18)		

the atom to which they were attached. Because of the low crystal quality and problems with disorder, refinement converged to a residual of 0.086. The final difference map shows some peaks of the order of 1 e Å^{-3} located in the region of the disordered tetraethylammonium group. These presumably reflect some residual disorder in this region. Selected bond angles and distances are presented in Table II.

Electrochemical Measurements. Cyclic voltammetry was performed under N_2 in CH_2Cl_2 (Aldrich Sureseal) with a supporting electrolyte of $[Bu_4N][ClO_4]$ (0.1 M, Fluka, vacuum dried at room temperature overnight) with a Princeton Applied Research Model 173/179 potentiostat/digital coulometer equipped with positive feedback IR compensation, a Model 175 universal programmer, and a Houston Instruments Model 2000 X-Y recorder. The electrochemical cell contained a 3-mm Pt disk working electrode, a Ag wire quasi-reference electrode, and a Pt foil counter electrode. Ferrocene (Fc) was added as an internal potential standard at the conclusion of each experiment. Formal potentials were calculated as the average of anodic and cathodic peak potentials and are reported vs NHE. Peak-to-peak separation of the Fc^+/Fc couple was similar to that of the iron-compound couples in all cases. Plots of peak current vs the square root of scan speed over the range 5–500 mV s^{-1} were found to be linear for all couples. Bulk electrolyses were performed under similar conditions in a standard three-compartment cell using Pt gauze working and counter electrodes and a Ag wire quasi-reference electrode.

Spectroscopic Methods. Infrared spectra were obtained on either Nicolet 5DXB or Mattson Galaxy Series 5000 FTIR spectrometers. UV/vis spectra were obtained on Perkin-Elmer Lambda Array 3840, Hewlett Packard 8451A, or IBM 9430 UV/visible spectrophotometers. Conventional X-band EPR spectra were recorded on a Bruker ER300 spectrometer equipped with an Oxford ESR-900 helium flow cryostat. Spin quantitations were performed as previously described under nonsaturating conditions using $CuClO_4$ as standard.[19] Integer-spin EPR spectra were recorded using a Varian E-109 spectrometer equipped with an E231 or E236 cavity, Oxford Instruments ESR-910 cryostat, and Hewlett Packard 436A power meter and 5350B microwave frequency counter. Spin quantitations were performed under nonsaturating conditions as previously described using crystals of Fe^{2+} doped into zinc fluorosilicate as standard.[13b,20] Mössbauer spectra were obtained on constant-acceleration instruments, and isomeric shifts are reported relative to an iron metal standard at 298 K.

Results

X-ray structural studies. X-ray crystal structures have been obtained for both $[Et_4N][Fe^{IV}Cl(\eta^4\text{-MAC*})]$[10d] and $[Et_4N]_2[Fe^{III}Cl(\eta^4\text{-MAC*})]\cdot CH_2Cl_2\cdot H_2O$. The structural analyses reveal that the iron complex in $[Et_4N][Fe^{IV}Cl(\eta^4\text{-MAC*})]$ is most appropriately considered to have C_{1h} symmetry, while the iron complex in $[Et_4N]_2[Fe^{III}Cl(\eta^4\text{-MAC*})]\cdot CH_2Cl_2\cdot H_2O$ has C_1 symmetry. An ORTEP drawing of the iron(III) complex is shown in Figure 1. The two distinct symmetries can be seen by examination of Figure 2, which shows the geometries and bond angles surrounding the two iron centers. Selected bond distances are presented in the caption to Figure 2 for $[Et_4N][FeCl(\eta^4\text{-MAC*})]$ and in Table II for $[Et_4N]_2[FeCl(\eta^4\text{-MAC*})]\cdot CH_2Cl_2\cdot H_2O$.

For the iron(IV) complex, the four nitrogen atoms lie in a plane where the dihedral angle between any two planes containing three of the atoms is 0°. The iron atom sits 0.42 Å out of the amide nitrogen plane. The iron and chlorine atoms lie in a mirror plane which, in Figure 2, is shown slightly tilted out of the plane of the paper so that all the nitrogen donor atoms can be seen. This symmetry plane also contains the quaternary carbon of the diethylmalondiamide unit and the ketone functionality in the macrocyclic ring. The bond angles at the iron atom all preserve the σ_h symmetry element, and at the 3σ confidence level, the mirror plane is also preserved by the Fe–N distances. The z-axis is properly placed perpendicular to the mirror plane and bisects the N–Fe–N angles of the five-membered rings above which it lies. The π-bonds of the amido-N ligands are arranged such that the malondiamide six-membered ring contains two amido-N π-bonds and the ketone ring contains none. The Fe–Cl bond is tilted away from the axis perpendicular to the amido-N plane toward the ketone six-membered ring and the amide π-bonds that lie in the five-membered rings. The low symmetry in the π-bonding system around the iron atom could be the cause of the Fe–Cl bond tilting and indicates that an approximation to higher order symmetry should not be made when considering the electronic structure.

For the iron(III) complex, $[Et_4N]_2[Fe^{III}Cl(\eta^4\text{-MAC*})]\cdot CH_2Cl_2\cdot H_2O$, a lower symmetry is indicated by the structural data (Figures 1 and 2). The mirror plane is no longer present as demonstrated by the different bond angles presented in Figure 2. At the 3σ confidence level, the Fe–Cl distance of 2.406(6) Å is clearly longer than for the corresponding bond of the iron(IV) complex of 2.309(3) Å, while the Fe–N_{av} bond distances are not significantly different for the iron(III) and iron(IV) compounds.

(19) (a) Aasa, R.; Vänngård, T. *J. Magn. Reson.* **1975**, *19*, 308–315. (b) Lipscomb, J. D. *Biochemistry* **1980**, *19*, 3590–3599.

(20) Hendrich, M. P.; Münck, E.; Fox, B. G.; Lipscomb, J. D. *J. Am. Chem. Soc.* **1990**, *112*, 5861–5865.

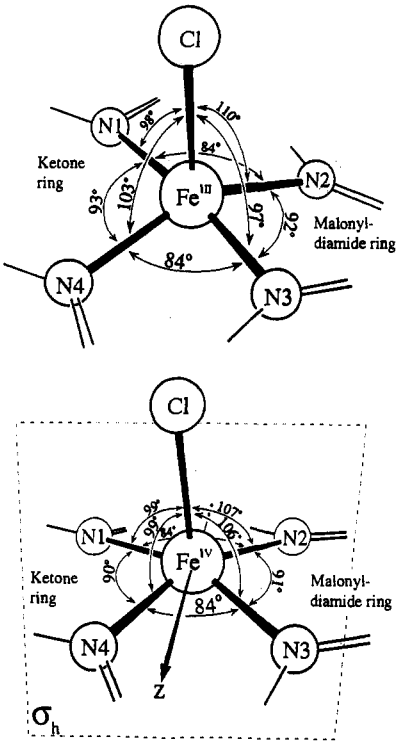

Figure 2. Diagrams showing immediate coordination sphere bond angles for $[Fe^{III}Cl(\eta^4\text{-MAC*})]^{2-}$ (top) and $[Fe^{IV}Cl(MAC*)]^{-}$ (bottom), illustrating symmetry properties for both complexes. Selected bond distances (Å) for $[Fe^{IV}Cl(\eta^4\text{-MAC*})]^{-}$ are as follows: Fe–Cl, 2.309(3); Fe–N1, 1.879(7); Fe–N2, 1.892(7); Fe–N3, 1.926(6); Fe–N4, 1.909(6).

The macrocyclic ligand system in the iron(III) case is significantly distorted when compared to that found in the iron(IV) complex. All the amido-*N* functional groups of the dianion $[Fe^{III}Cl(\eta^4\text{-MAC*})]^{2-}$ are significantly distorted from planarity,[21,22] and the likely source of the nonplanarities is a mismatch of the geometrical features of the macrocyclic ligand and the structural requirements of the iron(III) center. This type of nonplanarity for inorganic amido-*N* ligands has been found for a planar cobalt complex of the $[\eta^4\text{-MAC*}]^{4-}$ ligand.[22]

Electrochemistry and UV/Visible Spectroscopy. The cyclic voltammogram of $[Et_4N]_2[Fe^{III}Cl(\eta^4\text{-MAC*})]\cdot CH_2Cl_2$ is shown in Figure 3. One wave with a peak to peak separation of 144 mV is observed at $E_f = -65$ mV (vs Fc^+/Fc) (ca. 640 mV vs NHE). This value can be compared with the value of 770 mV for the Fe^{3+}/Fe^{2+} couple in water under standard conditions (CRC). Since the macrocyclic ligand system is devoid of delocalized π-bonding networks which can serve as the partial or complete site of oxidation, the low value of $E_f(Fe^{IV}/Fe^{III})$ can be attributed to the large σ-donor capacity of the amido-*N* donors, a point first clearly demonstrated by Margerum for copper peptide complexes[23] and found subsequently for copper(III) diamido-*N*-diphenoxido and diamido-*N*-dialkoxido compounds.[24] This factor suggests

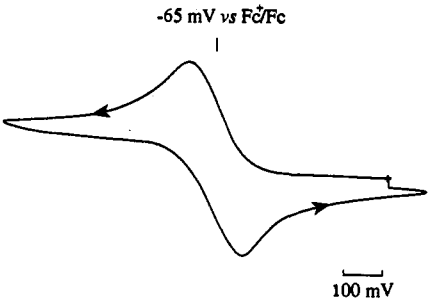

Figure 3. Cyclic voltammogram for the $[FeCl(\eta^4\text{-MAC*})]^{-/2-}$ couple measured in CH_2Cl_2 with 0.1 M $[Bu_4N][ClO_4]$ as supporting electrolyte. The cyclic voltammogram for the Fc^+/Fc internal standard is not displayed since it is nearly coincident with the $Fe^{IV/III}$ couple of the complex.

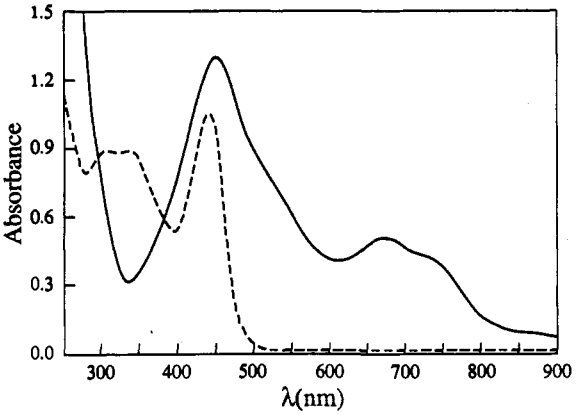

Figure 4. UV/visible spectrum of $[Et_4N]_2[Fe^{III}Cl(\eta^4\text{-MAC*})]$ (- - -, 0.13 mM) and $[Ph_4P][Fe^{IV}Cl(\eta^4\text{-MAC*})]$ (—, 0.12 mM) in CH_3CN.

one should anticipate a large covalency in the bonding of the tetraamido-*N* macrocycle to both the iron(IV) and iron(III) centers.

The UV/vis spectra of the $[Fe^{III}Cl(\eta^4\text{-MAC*})]^{2-}$ and the $[Fe^{IV}Cl(\eta^4\text{-MAC*})]^{-}$ anions in CH_3CN are shown in Figure 4. The iron(IV) complex exhibits a manifold of absorption bands with three clearly visible features at 450, 672, and 740 nm. In addition, the high-energy band has a shoulder in the vicinity of 530 nm. The most intense absorption for the iron(III) complex occurs at 440 nm, with two weaker bands at 335 and 310 nm. Because of a slow conversion of the iron(IV) anion to the iron(III) anion in CH_3CN, the molar absorptivies were calculated from measurements obtained from multiple, rapidly prepared solutions, each of which contained weighed portions of the iron(IV) crystals (20–40 mg). By this method, it was possible to obtain reproducible molar absorptivity values of $\epsilon_{450} = 10\,900 \pm 500$ L mol^{-1} cm^{-1} and $\epsilon_{672} = 4100 \pm 480$ L mol^{-1} cm^{-1} at the 3σ confidence level. In a similar study, the molar absorptivity of the iron(III) complex was determined to be $\epsilon_{440} = 7600 \pm 400$ L mol^{-1} cm^{-1}. We anticipate a more detailed study of the UV/vis spectra of both anions.

Mössbauer and EPR Studies. We have analyzed the Mössbauer and EPR spectra discussed below in the framework of the spin Hamiltonian

$$H = H_e + H_{hf} \quad (1)$$

$$H_e = D[S_z^2 - {}^1/_3S(S+1)] + E(S_x^2 - S_y^2) + \beta \mathbf{S}\cdot\mathbf{g}\cdot\mathbf{H} \quad (2)$$

$$H_{hf} = \mathbf{S}\cdot\mathbf{A}\cdot\mathbf{I} - g_n\beta_n\mathbf{H}\cdot\mathbf{I} + H_Q \quad (3)$$

$$H_Q = \frac{eQV_{z''z''}}{12}[3I_{z''}^2 - I(I+1) + \eta(I_{x''}^2 - I_{y''}^2)] \quad (4)$$

In eq 2, D and E are the principal values of the traceless zero field

(21) The twisted and the pyramidalization terms χ_C and χ_N were obtained from the primary torsion angle data ω_1, ω_2, and ω_3 as follows: $\tau = (\omega_1 + \omega_2)/2$; $\chi_N = (\omega_2 - \omega_3 + \pi) \bmod 2\pi$; $\chi_C = (\omega_1 - \omega_3 + \pi) \bmod 2\pi$. Here we used the modified twist angle, $\bar{\tau} = \tau \bmod \pi$. $\bar{\tau}$ maximizes at ±90° and can be interpreted as the angle between the idealized positions of the pπ orbitals on C and N. The pyramidalization terms maximize at ±60°. For the amido-*N* ligand at N1, $\tau = -27$, $\chi_N = -26$, $\chi_C = -2$; at N2, $\tau = -20$, $\chi_N = -15$, $\chi_C = -8$; at N3, $\tau = -6$, $\chi_N = -14$, $\chi_C = -6$; at N4, $\tau = 20$, $\chi_N = 18$, $\chi_C = -7$: (a) Dunitz, J. D.; Winkler, F. K. *J. Mol. Biol.* **1971**, *59*, 169. (b) Dunitz, J. D.; Winkler, F. K. *Acta Crystallogr., Sect. B: Struct. Crystallogr. Cryst. Chem.* **1975**, *B31*, 251. (c) Walshal, A.; Levitt, M.; Lifson, S. *J. Mol. Spectrosc.* **1970**, *33*, 84.

(22) Collins, T. J.; Uffelman, E. S. *Angew. Chem., Int. Ed. Engl.* **1989**, *28*, 1509–1511.

(23) Bossu, F. P.; Chellapa, K. L.; Margerum, D. W. *J. Am. Chem. Soc.* **1987**, *99*, 2195–2203.

(24) Anson, F. C.; Collins, T. J.; Richmond, T. G.; Santarsiero, B. D.; Toth, J. E.; Treco, B. G. R. T. *J. Am. Chem. Soc.* **1987**, *109*, 2974–2979.

Table III. Electronic and Hyperfine Parameters for $[Fe^{III}Cl(\eta^4\text{-MAC*})]^{2-}$ and $[Fe^{IV}Cl(\eta^4\text{-MAC*})]^{-}$ at 4.2 K

param	$[Fe^{III}Cl(\eta^4\text{-MAC*})]^{2-}$			$[Fe^{IV}Cl(\eta^4\text{-MAC*})]^{-}$		
spin		$^3/_2$			2	
D (cm^{-1})		−3.7(4)			−2.6(4)	
E/D		0.05(1)			0.14(3)	
	x	y	z	x	y	z
g[a]	2.03	2.03	2.06	1.84[b]	1.85[b]	1.80
				x'	y'	z'
$A/g_n\beta_n$ (T)	+5(8)	−22(1)	−16.6(2)	−18(1)[c]	−15(1)[c]	−10.8(2)[c]
ΔE_Q (mm/s)		−3.60(5)			+0.89(2)	
η		−3.7(5)[d]			−2.7(2)[e]	
δ (mm/s)		0.25(3)			−0.04(2)	
Γ^f (mm/s)		0.34			0.40	

[a] From EPR simulations. [b] Obtained from $g_{x,y} = g_z - 2D/\lambda(1 \mp E/D)$ using $g_z = 1.80$ and $\lambda = 129$ cm^{-1}. [c] Principal axis values quoted in the (x',y',z') frame of the A-tensor. The z'-axis is parallel to the electronic z-axis; x' and y' are obtained by rotating the electronic system by 70° around the z-axis. [d] In proper frame (x'',y'',z''), $\Delta E_Q = +3.6$ mm/s and $\eta = 0.15$. [e] Rotation of the electric field gradient into a proper axis frame gives $\Delta E_Q = -0.89$ mm/s and $\eta = 0.15$. [f] Full width at half-maximum of the Lorentzian line.

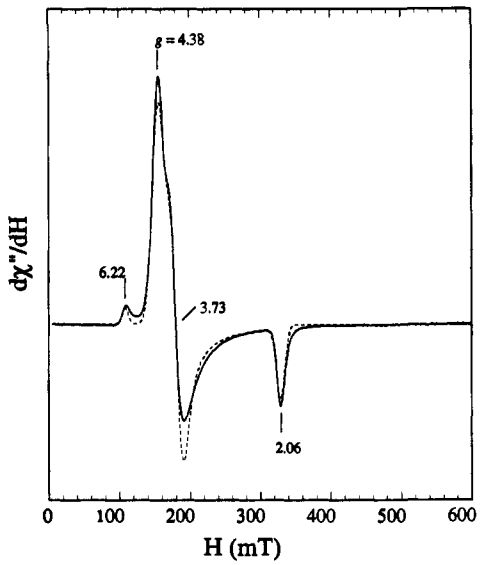

Figure 5. X-Band EPR spectrum of 28 mM $[Et_4N]_2[Fe^{III}Cl(\eta^4\text{-MAC*})]\cdot CH_2Cl_2$ in CH_3CN. Effective g-values are as marked. The dotted line is the sum of the contributions from the $M = \pm^1/_2$ and M = $\pm^3/_2$ doublets of an $S = {}^3/_2$ system. These simulations were generated with a program for an effective $S = {}^1/_2$ system using the procedures and effective g-values listed in the text. Instrumental parameters: 5 mW; gain 8000; center field 305 mT; scan range 600 mT; scan time 320 s; time constant 0.25 s; modulation amplitude 10 G; modulation frequency 100 kHz; 9.46 GHz; sample temperature ~5 K.

splitting (ZFS) tensor and **g** is the electronic g-tensor; for both compounds studied here the principal axis values of **g** are close to $g = 2$. In eq 3, A is the magnetic hyperfine tensor and H_Q describes the interaction of the quadrupole moment of the ^{57}Fe nucleus with the electric field gradient (EFG) tensor; this tensor has principal components $V_{x''x''}$, $V_{y''y''}$, and $V_{z''z''}$. We quote in Table III the components of the EFG-tensor in the coordinate frame of the ZFS-tensor; this choice requires that η can be outside the range $0 \le \eta \le 1$. In the conventional "proper" frame, $|V_{z''z''}| \ge |V_{y''y''}| \ge |V_{x''x''}|$, $0 \le \eta \le 1$ with $\eta = (V_{x''x''} - V_{y''y''})/V_{z''z''}$. At $T \le 4.2$ K, the electronic spins of both $[Fe^{III}Cl(\eta^4\text{-MAC*})]^{2-}$ and $[Fe^{IV}Cl(\eta^4\text{-MAC*})]^{-}$ were found to relax slowly compared to the nuclear precession times. Consequently, the low-temperature Mössbauer spectra have been simulated by assuming the slow fluctuation limit.

$[Fe^{III}Cl(\eta^4\text{-MAC*})]^{2-}$. An X-band EPR spectrum of $[Et_4N]_2[Fe^{III}Cl(\eta^4MAC*)]$ dissolved in CH_3CN is shown in Figure 5. This spectrum unambiguously identifies the spin of the ground multiplet. The major resonances at effective g-values of $g_x = 3.73$, $g_y = 4.38$, and $g_z = 2.06$ can be assigned to the $M = \pm^1/_2$ doublet of an $S = {}^3/_2$ system. Thus, for $E/D = 0.035$ and $g = (1.97, 2.08, 2.06)$, eq 2 predicts effective g-values $g_x'' = 3.73$, $g_y'' = 4.38$, and $g_z'' = 2.06$ for the $M = \pm^1/_2$ doublet and $g_x' = g_y' = 0.2$ and $g_z' = 6.19$ for the $M = \pm^3/_2$ levels. The effective g-values of the $M = \pm^3/_2$ level are typical of Kramers doublets having uniaxial magnetic properties; that is $g_z' \gg g_x'$, g_y'. Variable-temperature studies have revealed that the intensity of the $M = \pm^1/_2$ EPR spectrum increases with increasing temperature between 5 and 10 K, showing that the $M = \pm^1/_2$ levels are excited states. Hence, $D < 0$ in eq 2. Although the ground $M = \pm^3/_2$ doublet has a substantially higher population at 5 K (~90% according to the Mössbauer results described below) than the $M = \pm^1/_2$ doublet, the $g_z' = 6.22$ resonance has an intrinsically weaker intensity than the $g_y'' = 4.38$ and $g_x'' = 3.73$ excited-state resonances because g_x' and g_y' are small; the intensity of the $g_z' = 6.22$ resonance is proportional to $(g_x')^2 + (g_y')^2$.[19a] The dashed line in Figure 5 is the result of computer simulations of the $S = {}^3/_2$ EPR spectrum. The width of the EPR spectra of systems with $S \ge {}^3/_2$ is often dominated by contributions attributable to a distribution of the ZFS parameter E/D (E/D-strain). We have modeled the spectrum of the $M = \pm^1/_2$ doublet by assuming that E/D is normally distributed and have found that the features around $g = 4$ are well described by using the distribution width $\sigma_{E/D} = 0.05$. With the aid of eq 2, the $\sigma_{E/D}$ values were transformed into σ_{g_i} values (i = x, y, z) along the principal axes of the ZFS tensor and treated as a line width tensor in an $S = {}^1/_2$ simulation program. The σ_{g_z} thus derived produced a width of 6 mT at $g_z'' = 2.06$, which is substantially smaller than the 15 mT observed experimentally. Some of this mismatch can probably be attributed to unresolved ^{14}N hyperfine interactions of the electronic spin system with the four amide ligands. Since we have as yet no information on these transferred hyperfine interactions, the width at g_z'' was modeled by adjusting $\sigma_{g_z''}$ to match the width of the simulation of that of the experimental data. The resonance at $g_z' = 6.22$ originates from the $M = \pm^3/_2$ ground doublet. In order to model its width, a $\sigma_{g_z'}$ eight times larger than that used for the excited state doublet was required.[25] After adjustment of the intensities of both spectra with the Boltzmann factor, computed for $D = -3.7$ cm^{-1} obtained from Mössbauer spectroscopy, and application of the g_{av}^p corrections of Aasa and Vänngård,[19a] the computed spectra of the two doublets were added to give the dashed line of Figure 5. Overall, the agreement between theory and experiment is quite good.

Figures 6 and 7 show selected Mössbauer spectra of $[Et_4N]_2[Fe^{III}Cl(\eta^4\text{-MAC*})]$ recorded in the temperature range from 4.2 K to room temperature in fields up to 6.0 T. Figure 6A shows a Mössbauer spectrum of polycrystalline $[Et_4N]_2[Fe^{III}Cl(\eta^4\text{-MAC*})]$ recorded at 298 K. The spectrum consists of a

(25) It would be interesting to investigate the reasons for differences in the ground- and excited-state line widths with a more realistic line shape model for an $S = {}^3/_2$ system. The development of such a model is beyond the scope of this study.

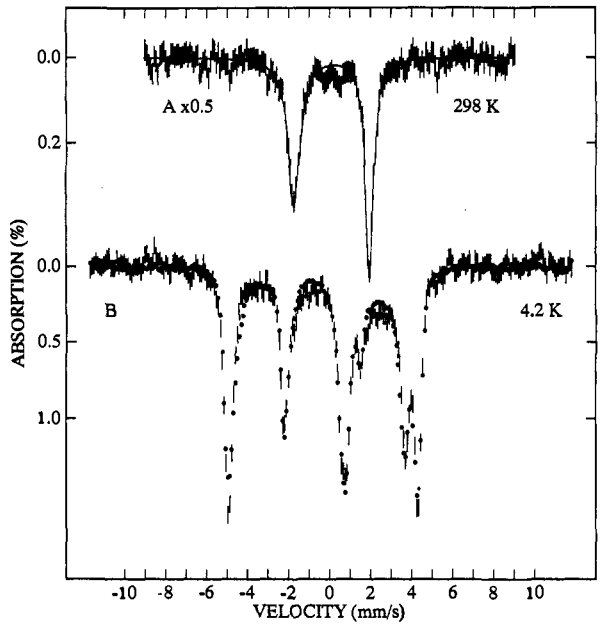

Figure 6. Mössbauer spectra of $[Et_4N]_2[Fe^{III}Cl(\eta^4\text{-MAC*})]\cdot CH_2Cl_2$ obtained in 50-mT magnetic field applied parallel to the propagation direction of the γ-rays; (A) Polycrystalline solid dispersed in adamantane (as a filler) at 298 K; (B) 4.2 K spectra of sample from (A) and of $[Et_4N]_2[Fe^{III}Cl(\eta^4\text{-MAC*})]\cdot CH_2Cl_2$ dissolved in CH_3CN (•). The solid line in (A) is a least-squares fit with Lorentzian lines having the following parameters: δ = 0.15 mm/s; ΔE_Q = 3.6 mm/s.

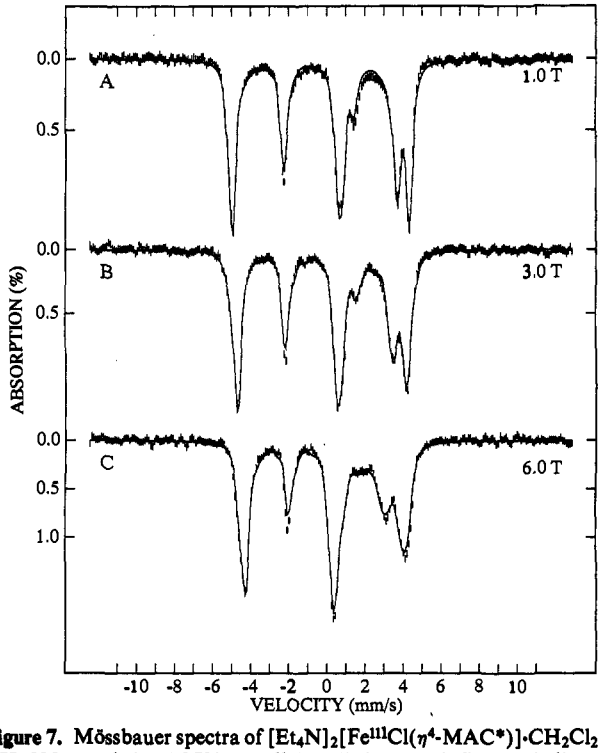

Figure 7. Mössbauer spectra of $[Et_4N]_2[Fe^{III}Cl(\eta^4\text{-MAC*})]\cdot CH_2Cl_2$ in CH_3CN recorded at 4.2 K in parallel applied magnetic fields as indicated. The solid lines are simulations generated from eq 1 for $S = {}^3/_2$ using the parameters listed in Table III.

quadrupole doublet with ΔE_Q = 3.68 mm/s and δ = 0.14 mm/s. The broader low-energy line shows that the electronic system has not yet reached the fast fluctuation limit at room temperature. Within the uncertainties, ΔE_Q is the same at 298 and 4.2 K (see Table III), demonstrating that no excited orbital state is measurably populated at room temperature. Figure 6B shows the 50-mT Mössbauer spectra of polycrystalline $[Et_4N]_2[FeCl(\eta^4\text{-MAC*})]$ and of $[Et_4N]_2[FeCl(\eta^4\text{-MAC*})]$ dissolved in CH_3CN. These spectra are essentially the same, showing that the ligand structure is not measurably perturbed upon dissolving the compound. This suggests that the axial chloride ligand present in the crystalline material is also likely to be present in solution.

The low-field Mössbauer spectra ($H \leq 1.0$ T, Figures 6B and 7A) recorded at 4.2 K exhibit a six-line absorption pattern. Such patterns are typically associated with Kramers doublets having uniaxial magnetic properties, in accord with the conclusions reached from EPR. Mössbauer spectra recorded at 1.5 K in a field of 50 mT were the same as those observed at 4.2 K, showing that the $M = \pm{}^1/_2$ doublet is not detectably populated at 4.2 K.

The magnetic splittings of the Mössbauer spectra are determined by the magnitude of the effective field, $|\mathbf{H}_{eff}| = |\mathbf{H}_{int} + \mathbf{H}|$, where $\mathbf{H}_{int} = -\langle \mathbf{S} \rangle \cdot \mathbf{A}/g_n\beta_n$ is the internal magnetic field. Owing to the uniaxial properties of the ground doublet, the internal field is directed along the z-direction defined by the ZFS interaction, with $\langle S_z \rangle \approx \pm 1.5$ for the two levels of the ground doublet. Consequently, A_z and the z-component of the EFG-tensor, V_{zz}, are determined at low fields. As the applied field is increased, the $M = \pm{}^1/_2$ levels are mixed into the ground state, resulting in appreciable values of $\langle S_x \rangle$ and $\langle S_y \rangle$. The extent of mixing depends on the magnitude of the ZFS parameter D and thus can be used for the determination of D.[26] At H = 8.0 T, the strongest field used in this study, only the $M = -{}^3/_2$ level is populated at 4.2 K. Under these conditions $\langle S_x \rangle$ and $\langle S_y \rangle$ of the lowest level approach the limit $\langle S_x \rangle = \langle S_y \rangle = -1.5$, and thus the spectra become sensitive to A_x and A_y.

The solid lines in Figure 7 are computer simulations generated by solving eqs 1–4 using the parameters quoted in Table III. The parameters quoted in Table III fit the spectra of the polycrystalline material and the frozen CH_3CN solution shown in Figure 6B as well. After suitable values for the parameters are found by simulations of the individual spectra, the final parameter set was obtained by simultaneously least-squares fitting the entire data set. It is noteworthy that the EFG- and A-tensors are collinear and nearly axial and that the symmetry axes of both tensors are in the xy plane of the ZFS tensor.

$[Fe^{IV}Cl(\eta^4\text{-MAC*})]^-$. We have studied samples of $[Fe^{IV}Cl(\eta^4\text{-MAC*})]^-$ both as a polycrystalline solid and as a frozen CH_3CN solution. The zero-field Mössbauer spectrum of a frozen solution is shown in Figure 8A. This 4.2 K spectrum consists of a fairly symmetric quadrupole doublet with ΔE_Q = 0.89 mm/s and δ = –0.04 mm/s. The same parameters were obtained for the polycrystalline material (Figure 9A); however, the absorption lines were narrower in the solid (0.32 mm/s vs 0.38 mm/s). We have previously suggested that this value of δ is indicative of the iron(IV) oxidation state.[10d] In the following, we will demonstrate that $[Fe^{IV}Cl(\eta^4\text{-MAC*})]^-$ contains high-spin (S = 2) iron(IV).

Figure 8B–D shows a series of high-field spectra obtained on $[Ph_4P][Fe^{IV}Cl(\eta^4\text{-MAC*})]$ dissolved in CH_3CN and enriched to 12% in ^{57}Fe.[27] The spectra shown in Figure 9B,C were obtained on a polycrystalline sample with the same counterion. The 1.0-T spectra of $[Ph_4P][Fe^{IV}Cl(\eta^4\text{-MAC*})]$ shown in Figures 8C and 9C display magnetic patterns consisting of six fairly sharp absorption lines. Such patterns result when the magnetic hyperfine field is fixed relative to the EFG-tensor for essentially all molecules in the sample. This situation arises when the electronic system is uniaxial at the temperature of measurement, i.e., when $\langle \mathbf{S} \rangle$ is large in one direction and essentially zero

(26) Another method of measuring D by Mössbauer spectroscopy involves increasing the temperature to affect a significant population of the $M = \pm{}^1/_2$ levels and then decomposing the spectra into contributions from the two Kramers doublets. Because of unfavorable electronic relaxation rates for T > 10 K, this method did not work for $[Et_4N]_2[Fe^{III}Cl(\eta^4\text{-MAC*})]$.

(27) For studies in strong applied fields, a ^{57}Fe concentration of 1–2 mM is desirable. Using samples with ^{57}Fe in natural abundance would then require a compound concentration of 40–80 mM. Such concentrations often lead to solubility or spin–spin relaxation problems. Synthesis of compounds with >90% enrichment is generally expensive and often unnecessary. We have found that an isotopic enrichment of ~10–15% is a good compromise.

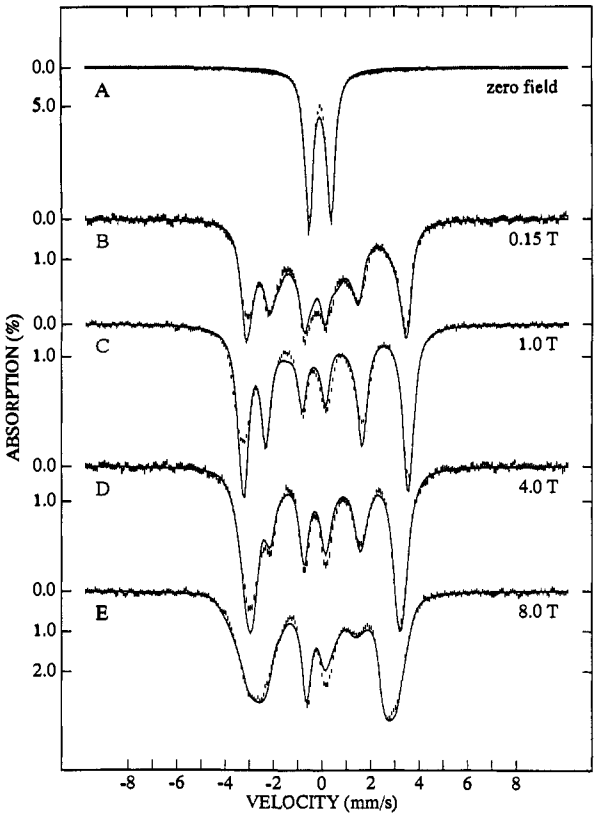

Figure 8. Mössbauer spectra of the ^{57}Fe-enriched $[Ph_4P][Fe^{IV}Cl(\eta^4\text{-MAC*})]\cdot C_6H_6$ in CH_3CN obtained at 4.2 K in the indicated parallel applied magnetic fields. The solid lines are simulations generated from eq 1 for $S = 2$ using the parameters listed in Table III.

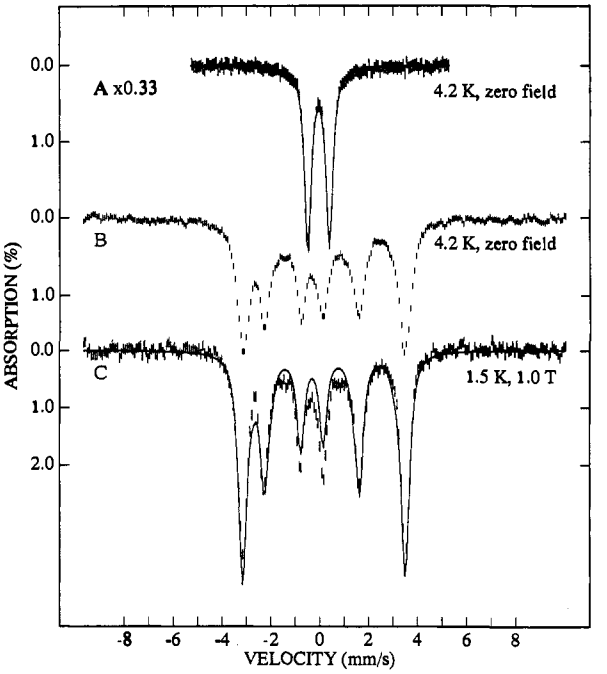

Figure 9. Mössbauer spectra of polycrystalline samples of $[Fe^{IV}Cl(\eta^4\text{-MAC*})]^-$ prepared with different counterions: (A) $[Bu_4N]^+$; (B, C) $[Ph_4P]^+$. The solid line in (A) line is a least-squares fit with Lorentzian lines having the following parameters: $\delta = -0.02$ mm/s; $\Delta E_Q = 0.99$ mm/s. The solid line in (C) was generated from eq 1 using the parameters listed in Table III.

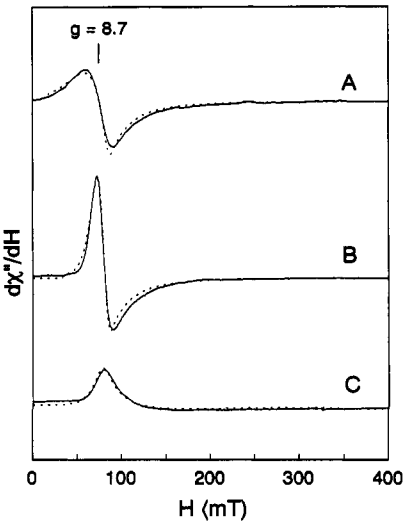

Figure 10. X-Band EPR spectra (—) and simulations (···) of (A) 2.5 mM $[Et_4N][Fe^{IV}Cl(MAC*)]$ in CH_3CN, $H_1 \parallel H$, (B) $[Et_4N][Fe^{IV}Cl(MAC*)]$ powder, $H_1 \parallel H$, and (C) as in (B), $H_1 \perp H$. Simulation parameters: (A) $D = -2.6$ cm^{-1}, $E = -0.41$ cm^{-1}, $\sigma_E = 0.06$ cm^{-1}, $g_z = 1.80$; (B, C) $D = -2.5$ cm^{-1}, $E = -0.38$ cm^{-1}, $\sigma_E = 0.04$ cm^{-1}, $g_z = 1.80$. Instrumental parameters: 0.02 mW; gain, (A) 10 000; modulation amplitude 1 mT; modulation frequency 100 kHz; 9.1 GHz; sample temperature 2.6 K.

perpendicular to this direction. While such situations occur frequently for Kramers doublets (as discussed above for $[Et_4N]_2[Fe^{III}Cl(\eta^4\text{-MAC*})]$), they also occur for systems with integer electronic spin having ZFS parameters such that the two lowest spin levels are nearly degenerate.[28] The six-line patterns of Figure 8 can be observed in magnetic fields as low as 0.1 T. This proves that the electronic spin relaxation rate at 4.2 K is significantly slower than the nuclear precession rate (~30 MHz). Since the zero-field Mössbauer spectrum of Figure 8A lacks magnetic interactions, it then follows that $[Fe^{IV}Cl(\eta^4\text{-MAC*})]^-$ has integer electronic spin.[29]

The X-band EPR spectra of $[Fe^{IV}Cl(\eta^4\text{-MAC*})]^-$ also show the presence of an integer spin system. Signals of systems with half-integral spin vanish when the oscillatory field, H_1, fluctuates parallel to the static field, H, but the signals of Figure 10 intensify as expected for an integer spin system[13] (for a discussion of the connection between the Mössbauer and EPR spectra of integer spin systems, see ref 13a). The temperature dependence of the $g_{eff} = 8.0$ signal indicates that it originates from a ground spin "doublet". Moreover, the position of the resonance is strongly suggestive of $S = 2$, based on the relation $g_{eff} \approx 4S$ (see below). This relation is approximate and does not rule out the possibility that $S = 1$; however, the $S = 1$ case can be eliminated both by quantitative EPR analysis and by the magnetic field dependence of the Mössbauer spectra discussed below. Thus, we will illustrate the magnetic properties of $[Fe^{IV}Cl(\eta^4\text{-MAC*})]^-$ with the $S = 2$ energy level scheme of Figure 11. The Mössbauer spectra of Figures 8 and 9 and the EPR spectra of Figure 10 are determined by the properties of the two lowest spin levels. Using the standard representation $|S,M\rangle = |2,M\rangle = |M\rangle$, the eigenstates of these levels are in good approximation given by[13b]

$$|2^s\rangle = (|+2\rangle + |-2\rangle)/\sqrt{2} \quad (5)$$

$$|2^a\rangle = (|+2\rangle - |-2\rangle)/\sqrt{2} \quad (6)$$

In zero magnetic field, the two lowest levels are split by $\Delta \approx 3D(E/D)^2$ and the expectation values of the electronic spin, $\langle S\rangle$, are zero for all five spin levels. In applied fields of moderate strength, i.e. for $\Delta \ll \beta H \ll |D|$, the z-component of the applied field mixes the two levels imparting a finite expectation value

(28) (a) Papaefthymiou, V.; Girerd, J.-J.; Moura, I.; Moura, J. J. G.; Münck, E. *J. Am. Chem. Soc.* **1987**, *109*, 4703–4710. (b) Zimmermann, R.; Huynh, B. H.; Münck, E. *J. Chem. Phys.* **1978**, *69*, 5463–5467.

(29) A Kramers system with slow spin relaxation would exhibit magnetic hyperfine interactions in zero field. For example, the zero-field spectra of $[Fe^{III}Cl(\eta^4\text{-MAC*})]^{2-}$ are similar to the 50-mT spectra shown in Figure 6.

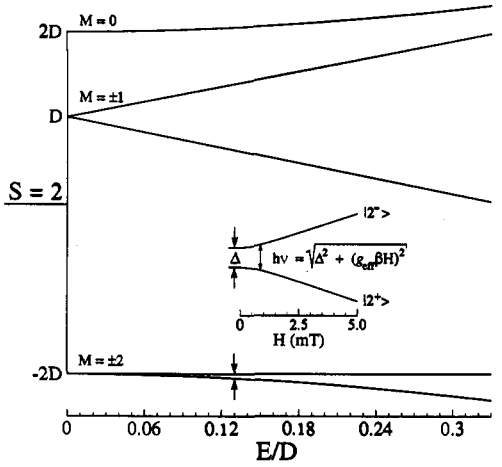

Figure 11. Energy levels of an $S = 2$ multiplet according to eq 2 for $H = 0$ and $D < 0$ as a function of the rhombicity parameter E/D. The value of E/D for which the integer spin EPR resonance is observed for $[Fe^{IV}Cl(MAC^*)]^-$ is indicated by the arrows. The insert shows the field dependence of the ground doublet for $E/D = 0.13$, for H applied along the z-axis.

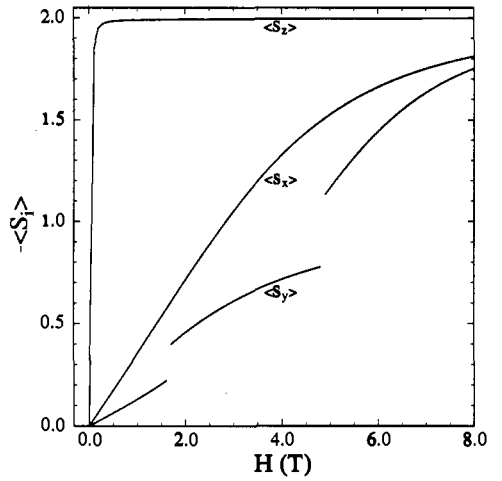

Figure 12. Spin expectations values $\langle S_i \rangle$ for the *lowest* level of $[Fe^{IV}Cl(MAC^*)]^-$ as a function of magnetic field calculated from eq 2 using the parameters quoted in Table III. The discontinuities in $\langle S_y \rangle$ are caused by level crossings when the magnetic field is applied along the y-direction.

$\langle S_z \rangle$ and thus an internal field $H_{int}(z) = -\langle S_z \rangle A_z/g_n\beta_n$ (the relevant matrix elements are $\langle 2^a|S_z|2^a\rangle = 2$ and $\langle 2^a|S_{x,y}|2^a\rangle = 0$). For moderate applied fields and $T \leq 4.2$ K, the Mössbauer spectra are determined by the properties of the two lowest spin levels. Figure 12 shows a plot of the expectation values $\langle S_x \rangle$, $\langle S_y \rangle$, and $\langle S_z \rangle$ for the *lowest* spin level. A similar plot is obtained for the other level except that the signs of the $\langle S_i \rangle$ are positive. The initial slope of $\langle S_z \rangle$ versus H is $-8g_z\beta/\Delta$, and thus, Mössbauer studies in small applied fields can be used to determine Δ. As can be seen from Figure 12, $\langle S_z \rangle$ and, correspondingly, the internal field $H_{int}(z)$ has reached 95% of the saturation value for $H = 0.15$ T. By analyzing the splitting patterns of the low-field spectra, we obtained $\Delta = 0.16 \pm 0.02$ cm^{-1}, $E/D = 0.13 \pm 0.03$, $A_z/g_n\beta_n = -10.6$ T, $\Delta E_Q = +0.89$ mm/s, and $0.05 \leq \eta < 0.2$.

One comment is in order at this point. The spectra of Figure 8B,C are essentially of the uniaxial type; they reflect a situation where an internal magnetic field is fixed relative to the EFG-tensor for all orientations of the molecules. Under these conditions, there exists an ambiguity in that a family of related values for the asymmetry parameter η and spherical polar angles α and β (which describe the orientation of H_{int} relative to the EFG-tensor) will produce identical powder Mössbauer spectra. We have analyzed the spectra using the method described by Zimmermann et al.[30] and have found that β is confined to $87° < \beta < 93°$ and that $0.05 \leq \eta < 0.2$. Thus, β and η are essentially determined; since $\beta \approx 90°$, the internal magnetic field H_{int} and the electronic z-axis are in the $x''y''$-plane of the EFG-tensor.

In strong applied magnetic fields, $\langle S_x \rangle$ and $\langle S_y \rangle$ approach their saturation values and the spectra become sensitive to A_x and A_y. Lines 2 and 5 of the 1.0-T spectra of Figures 8 and 9 are nuclear $\Delta m = 0$ transitions. In the limit $\beta H \gg |D|$, the intensities of these lines are essentially quenched. From a study of the intensities of $\Delta m = 0$ lines as the function of the applied field, the ZFS parameter D can be estimated. From an analysis of the high-field spectra, a value of $D = -2.6 \pm 0.4$ cm^{-1} has been obtained.

The solid lines in Figure 8 are spectral simulations generated by solving eq 1 for a sample containing randomly oriented molecules. The parameter set determined by these simulations is presented in Table III. Overall, the fits describe the complete set of spectra very well. There is a slight mismatch of the intensities in the central part of all high-field spectra, however. This mismatch can most probably be attributed to those molecules of the sample which are oriented such that the applied field is close to the electronic xy-plane. For such orientations, the two lowest spin levels are separated in energy by less than 4 cm^{-1} even in an applied field of 8.0 T. For these molecules, the electronic spin appears to be in the intermediate relaxation regime, a condition which causes a partial collapse of the magnetic pattern with an accumulation of intensity in the central part of the spectrum. Such orientation-dependent relaxation, which has been noted for other complexes,[31] necessarily places some constraints on the accuracy of the spectral simulations. Nevertheless, it became clear to us that the shapes of the spectra of Figure 8 cannot be properly simulated unless the A-tensor is allowed to be rotated relative to the frame of the ZFS-tensor. We have generated hundreds of simulated spectra before arriving at a parameter set which described the data set reasonably well. The parameters were then further refined by simultaneously least-squares fitting the set of spectra displayed in Figure 8.

The spectra shown in Figure 9 were obtained with polycrystalline material prepared with different counterions. The 4.2 K zero-field spectrum of $[Bu_4N][Fe^{IV}Cl(\eta^4\text{-}MAC^*)]$ shown in Figure 9A consists of a well-defined quadrupole doublet. In contrast, when $[Ph_4P]^+$ is used as a counterion, a magnetic pattern is observed even in zero applied field, showing that the material is magnetically ordered at 4.2 K (see Figure 9B).[32] The solid line drawn through the spectrum of Figure 9C was generated with the same parameters as the spectra of the solution sample shown in Figure 8, except for $\Delta E_Q = 0.99$ mm/s. As noted for the iron(III) state discussed above, the spectra obtained for frozen-solution samples were very similar to those observed for polycrystalline material.

The properties of integer spin doublets are dominated by ZFS interactions, resulting in dramatic changes in the EPR spectra relative to the spectra of compounds with half-integral spin. Integer spin EPR spectra can be quantified through three properties. First, the resonance condition for integer spin doublets with the field along the z-direction[13b] is

$$h\nu = \sqrt{\Delta^2 + (g_{eff}\beta H)^2} \qquad (7)$$

where $g_{eff} = 2Sg_zf$ and the factor f depends on S and E/D. For the $|2^a\rangle, |2^a\rangle$ doublet considered here, $f \approx 1 - {}^3/_8(E/D)^2$, and thus as E/D approaches zero, $f = 1$ and $g_{eff} \approx 8$ ($f = 0.99$ for the present case). Second, the selection rule for allowed transitions

(30) Zimmermann, R.; Münck, E.; Brill, W. J.; Shah, V. K.; Henzel, M. T.; Rawlings, J.; Orme-Johnson, W. T. *Biochem. Biophys. Acta* **1978**, *537*, 185–207.

(31) Zimmermann, R. H.; Spiering, H.; Ritter, G. *Chem. Phys.* **1974**, *4*, 133–141.

(32) In a preliminary study, we have determined that $[Ph_4P][Fe^{IV}Cl(\eta^4\text{-}MAC^*)]$ orders at ca. 9 K.

within the $|2^s\rangle$, $|2^a\rangle$ doublet is $\Delta M = 0$ and not $\Delta M = \pm 1$ as for Kramers systems. Third, the line shape of integer spin doublets is dominated by a spread in the splitting Δ due to spreads in the ZFS parameters D and E/D. These parameter distributions presumably arise from small structural variations of the metal site. These structural variations affect the orbital states and, via spin–orbit coupling, cause distributions in the ZFS parameters. As shown in Figure 10, the EPR spectra of $[Fe^{IV}Cl(\eta^4\text{-MAC}^*)]^-$ are broader for frozen solutions than for polycrystalline material, suggesting that additional strains develop at the interface of the compound with the solvent upon freezing.

The convolution of the ZFS distributions and the quadratic resonance condition necessitates computer simulation of the spectra to determine the ZFS energies and sample concentrations.[13b,20] The simulations of the integer spin EPR spectra of $[Fe^{IV}Cl(\eta^4\text{-MAC}^*)]^-$ shown in Figure 10 were generated by solving eq 2 for the parameters $D = -2.6$ cm^{-1}, $E = -0.41$ cm^{-1}, and $\sigma_E = 0.06$ cm^{-1}, with D taken from the Mössbauer results. These simulations require that $\Delta = 0.19$ cm^{-1}, in excellent agreement with $\Delta = 0.16$ cm^{-1} determined from the Mössbauer data. Morever, the EPR simulations also require that $g_z \approx 1.80$; the EPR spectra are insensitive to g_x and g_y. Quantitation of the signal of Figure 10A gave an $S = 2$ concentration of 2.8 mM, which is 12% higher than the concentration determined by optical spectroscopy, confirming that the signal represents essentially all iron of the sample and not some impurity.

We have considered the possibility that the EPR signal might originate from intermediate-spin ($S = 1$) iron(IV). Using again the spin Hamiltonian approximation, a reasonable simulation of the spectrum of Figure 10A was obtained for $D = -3.6$ cm^{-1}, $E = -0.14$ cm^{-1}, $g_z = 2.0$, and $\sigma_E = 0.006$ cm^{-1}. However, the spin concentration determined on the basis of this simulation was a factor of 2 lower than the concentration determined optically. Moreover, the assumption of $S = 1$ requires $\Delta = 0.28$ cm^{-1}, which is in severe conflict with the Mössbauer result, and a ratio $\sigma_E/E = 0.04$, which is nearly 1 order of magnitude smaller than the ratios we have observed for a variety of other metal complexes. Finally, the $S = 1$ complexes[10a] of $[Fe^{IV}Cl(\eta^4\text{-MAC}^*)]^-$ have substantially larger values for D (>20 cm^{-1}) and ΔE_Q (>3 mm/s). We thus conclude that the data are not compatible with an $S = 1$ assignment.

Discussion

Two oxidation states of the macrocyclic tetraamido coordination complex $[FeCl(\eta^4\text{-MAC}^*)]^{n-}$ have been studied here with Mössbauer and EPR spectroscopy. In the ferric state, the complex has an electronic ground state with intermediate-spin, $S = {}^3/_2$. Upon oxidation, the complex becomes high-spin iron(IV), $S = 2$, a spin state previously not reported for any isolated iron(IV) coordination complex. In the following, we discuss some of the pertinent features of our results.

The EPR spectrum of Figure 5 shows unambiguously that $[Fe^{III}Cl(\eta^4\text{-MAC}^*)]^{2-}$ has an $S = {}^3/_2$ ground state. With the exception of some iron(III) porphyrins,[14b,c] halobis(dialkyldithiocarbamato)iron(III) complexes,[14d-f] and some tetraaza macrocyclic iron(III) complexes,[33] iron(III) compounds are either low-spin ($S = {}^1/_2$) or high-spin ($S = {}^5/_2$). Moreover, most of the intermediate-spin heme complexes are not in a pure $S = {}^3/_2$ spin state but occur in a quartet/sextet mixed-spin form. The ground-state properties of the porphyrin complexes have been described in an electronic model proposed by Maltempo.[14a] Although it fails to account for the large quadrupole splittings of the porphyrins studied, this model has been quite successful in describing the magnetic properties of the electronic ground manifold. In particular, Maltempo has shown that the effective g-values are a very sensitive indicator for the presence of spin-admixed states. The g-values reported here suggest strongly that $[Fe^{III}Cl(\eta^4\text{-MAC}^*)]^{2-}$ has a pure $S = {}^3/_2$ ground state. This conclusion is supported by the observation of a large and temperature-independent quadrupole splitting, a property also considered to be a good index for the purity of the $S = {}^3/_2$ spin state.[14b,c]

Inspection of the parameters quoted in Table III shows that the magnetic hyperfine tensor of $[Fe^{III}Cl(\eta^4\text{-MAC}^*)]^{2-}$ has substantial anisotropy. The high-field Mössbauer spectra of Figure 7 establish unambiguously that the two major components of the A-tensor are negative and that the minor component is positive. Since the g-values are close to $g = 2.0$, the orbital contributions to the A-tensor can be assumed to be small, and we thus attribute the anisotropy to the spin-dipolar term. Since the latter is traceless, the contact contribution can be obtained by averaging the principal components of A. Our value $A_c/g_n\beta_n = -11.3$ T compares well with $A_c/g_n\beta_n = -11.9$ T obtained for the tetraphenylporphyrin complex $[Fe(TPP)(FSbF_5)][C_6H_5F]$, which has an almost pure $S = {}^3/_2$ ground state (see Table I of ref 14b).[34] Wickman and collaborators[14d-f] have reported substantially larger contact interactions for dithiocarbamate complexes, $A_c/g_n\beta_n \approx -22$ T. However, due to the uniaxial nature of the electronic ground state of the dithiocarbamate complexes, these authors were able to determine only the component of the A-tensor along the electronic z-axis, and they computed the contact interaction by assuming that A was isotropic.

The EFG-tensor of $[Fe^{III}Cl(\eta^4\text{-MAC}^*)]^{2-}$ is nearly axial. In Table III, this tensor is quoted in the electronic (xyz)-coordinate frame. Alternatively, the EFG is characterized by $\Delta E_Q = +3.66$ mm/s and $\eta = 0.14$ in conventional notation, where $|V_{z'z'}| \geq |V_{y'y'}| \geq |V_{x'x'}|$ assures $0 \leq \eta \leq 1$. The largest component of the roughly axial EFG-tensor is in the xy-plane of the ZFS tensor, a situation similar to that reported for iron(III)–dithiocarbamates.[14f] The A-tensor is roughly axial as well and its "symmetry" axis is parallel to the major component of the EFG. Since $E/D = 0.05$, the electronic system is nearly axial and thus the shapes of the calculated spectra are not sensitive to a *joint* rotation of both the A- and EFG-tensors around the z-axis of the ZFS tensor. Because of the low point symmetry of $[Fe^{III}Cl(\eta^4\text{-MAC}^*)]^{2-}$, we have considered the possibility that the principal axis frames of the various tensors are related to each other by rotations other than 90°. On the basis of an extensive set of simulations, we have concluded that the principal axes of the A- and EFG-tensors are aligned and that the z-axis of the ZFS-tensor is colinear with the z-axis of both hyperfine tensors.

In summary, the hyperfine parameters obtained for $[Fe^{III}Cl(\eta^4\text{-MAC}^*)]^{2-}$ are remarkably similar to those reported for $[Fe(TPP)(FSbF_5)][C_6H_5F]$, the only heme complex with an essentially pure $S = {}^3/_2$ ground state.[14b,c] The electronic structure of intermediate-spin ferric complexes is still poorly understood, and additional computational studies would be highly desirable. Theoretical studies must be directed toward understanding the origin of the large quadrupole splittings as well as the remarkably small contact interactions.

Oxidation of $[Fe^{III}Cl(\eta^4\text{-MAC}^*)]^{2-}$ yields a high-spin iron(IV) compound. Three arguments support this assignment. First, the material designated as $[Fe^{IV}Cl(\eta^4\text{-MAC}^*)]^-$ is obtained from the ferric $S = {}^3/_2$ form by a 1-electron oxidation as shown by controlled-potential coulometry. The comparatively anodic formal potential obtained by cyclic voltammetry, 640 mV vs NHE, strongly suggests the oxidation site involves the metal rather than being centered on the oxidation resistant ligands. Second, the −0.22 mm/s change in isomer shift attending this oxidation and the observed value of $\delta = -0.04$ mm/s for the oxidation product strongly supports an iron(IV) assignment.[35] Finally, the identification of the oxidized compound as an integer spin system by Mössbauer spectroscopy and the observation of an integer spin

(33) Koch, S.; Holm, R. H.; Frankel, R. B. *J. Am. Chem. Soc.* **1975**, *97*, 6714–6723.

(34) These authors quote A_c for the nuclear excited state. To obtain the A-values for the nuclear ground state, the values quoted in ref 14c have to be multiplied by the ratio of the nuclear magnetic moments; $g_g/g_e = -1.71$.

resonance with a g_{eff} characteristic of an $S = 2$ multiplet completes the proof that the compound is high-spin iron(IV). As discussed below, the set of magnetic hyperfine parameters suggests substantial covalency for the iron(IV) site.

Although $[Fe^{IV}Cl(\eta^4\text{-MAC*})]^-$ is apparently the first isolated high-spin iron(IV) compound,[35] tetravalent high-spin iron(IV) has also been observed in the extended lattices of mixed oxides with a perovskite structure.[12] The assignment of a high-spin state in the mixed oxides is primarily based on susceptibility measurements. These compounds have a $M_{0.5}La_{1.5}Li_{0.5}Fe_{0.5}O_4$ composition with iron surrounded by an elongated octahedron of oxygens and M = Ca, Sr, or Ba. The strong axial distortions (equatorial Fe–O = 1.85 Å; axial Fe–O = 2.25 Å for M = Sr) in these mixed oxides leads to the stabilization of the $^5A_{1g}$ ground state.

The $S = 2$ manifold of $[Fe^{IV}Cl(\eta^4\text{-MAC*})]^-$ has ZFS parameters such that an integer-spin EPR transition can be observed at low temperature. Quantitative analyses of the $g_{eff} = 8.0$ resonance shows that the EPR signal represents the majority of iron in the sample and not a minor impurity. The spectral simulations shown in Figure 10 also require that $g_z \approx 1.8$. Since the spin–orbit coupling constant λ, in $\lambda L\cdot S$, is positive for ions with a less than half-filled d shell, g_i values smaller than the free electron g-value are expected for high-spin iron(IV). The best simulations to the EPR spectra of Figure 10 were obtained for $g_z = 1.80$; however, slightly larger g_z values, $1.80 < g_z < 1.90$, cannot be ruled out. The quadrupole splitting of $[Fe^{IV}Cl(\eta^4\text{-MAC*})]^-$ is independent of temperature showing that the ground state consists of an orbital singlet well separated in energy from the first excited orbital state. This suggests that the ZFS- and g-tensors can be computed by a second-order perturbation treatment similar to that commonly used for the complementary high-spin iron(II) configuration. In this approach, g_x and g_y can be expressed by g_z and the ZFS parameters D and E; thus, $g_y = g_z - 2/\lambda(D + E)$ and $g_x = g_z - 2/\lambda(D - E)$.[31] Using the free ion value[36] $\lambda = 129$ cm^{-1}, and the ZFS parameters of Table III, values of $g_x = 1.84$ and $g_y = 1.85$ were obtained. In principle, these g-values could be checked by Mössbauer studies in strong applied fields at temperatures for which the electronic relaxation rate is fast compared to the nuclear precession frequencies. However, the compounds studied here do not attain the fast fluctuation limit even at 200 K.

The spectra calculated with the parameter set of Table III and shown in Figure 8 describe the experimental data obtained for $[Fe^{IV}Cl(\eta^4\text{-MAC*})]^-$ very well. These fits have yielded the first determination of the A-tensor for a high-spin iron(IV) complex. For symmetries not lower than rhombic, the components of the magnetic hyperfine tensor can be written as

$$A_i = P\{(g_i - 2) + {}^3/_{14}l_{ii} - \kappa\} \qquad (8)$$

where $P = 2g_n\beta_n\beta\langle r^{-3}\rangle$, $l_{ii} = \langle d|\{L_i^2 - L(L+1)/3\}|d\rangle$, and $|d\rangle$ designates the orbital ground state. The $(g_i - 2)$ term reflects the orbital contribution, the term involving l_{ii} has spin-dipolar origin, and κ describes the isotropic Fermi contact interaction. Spin-polarized Hartree–Fock calculations by Freeman and Watson suggest that $P/g_n\beta_n = 63$ T and that $P\kappa/g_n\beta_n = 27.5$ T for the free Fe^{2+} ion and $P/g_n\beta_n = 79$ T for the free Fe^{4+} ion.[37] Analyses of a series of distinct high-spin ferrous compounds by Varret have indicated that covalency can reduce P and κ by as much as 40%.[38] We are not aware of any theoretical studies of the Fe^{4+} contact interaction. However, Hartree–Fock calculations of Mn ions indicate that the contact interaction does not decline more than 20% in the series Mn^+, Mn^{2+}, Mn^{3+}.[37] The theoretical work thus suggests that, in the ionic limit, the ^5D configurations of iron(II) and iron(IV) produce EFG- and A-tensors of comparable magnitude.

By an averaging of the components of the A-tensor of $[Fe^{IV}Cl(\eta^4\text{-MAC*})]^-$, $A_{av}/g_n\beta_n = (A_x + A_y + A_z)/3g_n\beta_n = -14.6$ T, the traceless spin-dipolar contribution cancels. For high-spin ferrous ions, the orbital contribution opposes the contact term. In contrast, because high-spin iron(IV) has $(g_i - 2) < 0$, the orbital contribution has the same sign as the contact term for the iron(IV) species. Thus, the magnitude of the contact term is actually considerably smaller than 14.6 T. By using the Fe^{4+} free ion value for P determined by Freeman and Watson[37] and the value for $\kappa = 0.35$, found to be appropriate for a large number of iron(II) and iron(III) compounds,[39] an upper (ionic) range for $|A_{av}/g_n\beta_n| \approx 35$–40 T is obtained. Thus, it is apparent that the values of P and κ used for $[Fe^{IV}Cl(\eta^4\text{-MAC*})]^-$ need to be reduced substantially to account for the observed $A_{av}/g_n\beta_n$.

We mentioned that the Maltempo model[14a] for $S = {}^3/_2$ spin iron(III) hemes describes the magnetic properties of intermediate-spin hemes quite well. By application of this model to the approximately axial magnetic hyperfine tensor of $[Fe^{III}Cl(\eta^4\text{-MAC*})]^{2-}$ (setting $A_y + A_z = 2A_\perp$) and by use of eq 6 of ref 14c, the values $P/g_n\beta_n = 42$ T and $\kappa = 0.25$ for $[Fe^{III}Cl(\eta^4\text{-MAC*})]^{2-}$ can be calculated. By using these calculated values and the g-values listed in Table III, we calculate $A_c/g_n\beta_n = -17.6$ T for $[Fe^{IV}Cl(\eta^4\text{-MAC*})]^-$, close to the $A_{av}/g_n\beta_n$ value of −14.8 T determined above. This rough estimate suggests that the iron(III) and iron(IV) forms of $[FeCl(\eta^4\text{-MAC*})]^{n-}$ exhibit similar degrees of covalency. The observation of small hyperfine interactions is not a peculiarity of the H_4[MAC*] ligand. In fact, Demazeau and co-workers have reported hyperfine fields of $|H_{hf}| \approx 15$ T for the magnetically ordered phases of the high-spin iron(IV) mixed-oxides.[12] These hyperfine fields are substantially smaller that the fields observed along the direction of the *smallest* A-tensor component for $[Fe^{IV}Cl(\eta^4\text{-MAC*})]^-$, $H_{hf} = 2A_z/g_n\beta_n = -21.6$ T.

As judged by the electrochemical properties, the small magnetic hyperfine interactions, and the small quadrupole splitting, bonding to the iron(IV) ion in $[Fe^{IV}Cl(\eta^4\text{-MAC*})]^-$ is rather covalent, almost certainly a consequence of the Fe–N bonding. Interestingly, small values for ΔE_Q (0.8–1.3 mm/s) have also been reported for the high-spin mixed-oxide iron(IV) complexes mentioned above.[12] These small values of ΔE_Q suggest substantial covalencies, a suggestion supported by an examination of the magnetic hyperfine interactions for $[Fe^{IV}Cl(\eta^4\text{-MAC*})]^-$. Since these interactions are substantially smaller than expected for ionic complexes, considerable care must be exercised in analyzing the data by simple ligand field models. Since these models contain a considerable number of adjustable parameters, it seems prudent to postpone such analyses until results from complementary techniques become available.

Our findings of a considerable covalency in the amido-*N*–iron bonding for both iron(III) and iron(IV) anions are not unexpected on the basis of published evidence indicating that amido-*N* ligands have a comparatively high σ-donor capacity, a property that tracks with a high pK_a for the conjugate acid of any given ligand.[23] Thus, in the bonding levels of amido-*N* complexes, the metal d-orbitals can be expected to have greater than usual ligand admixtures where symmetry allows, resulting from the comparatively high energy for the nitrogen σ-donor lone pairs of the

(35) Koikawa et al. have recently reported that $[Pr_4N]_2[Fe(L)_2]\cdot 2H_2O$, with L = *N*-(2-hydroxyphenyl)salicyclamide, has a high-spin iron(IV) configuration. This conclusion was based upon the quoted value of $\mu_{eff} = 4.99$ μ_B at 298 K. However, the 298 K Mössbauer parameters, $\Delta E_Q = 0.56$ mm/s and $\delta = 0.40$ mm/s, conflict with an iron(IV) assignment; in fact, the parameters are strongly suggestive of the iron(III) state. Moreover, the quoted $E°$ for the iron(IV/III) couple of this complex was −0.13 V, i.e., 0.53 V more negative than the iron(IV/III) couple of the tetraamido-*N* complex $[FeCl(\eta^4\text{-MAC*})]^{n-}$: Koikawa, M.; Okawa, H.; Maeda, Y.; Kida, S. *Inorg. Chim. Acta* **1992**, *194*, 75–79.

(36) Abragam, A.; Bleaney, B. In *Electron Paramagnetic Resonance of Transition Ions*; Oxford University Press: New York, 1986.

(37) Freeman, A. J.; Watson, R. E. In *Magnetism*; Rado, G. T., Suhl, H., Eds.; Academic Press: New York, 1965; Vol. IIA, pp 167–305.

(38) Varret, F. *J. Phys. Coll. C6* **1976**, *37*, 437–456.

(39) Lang, G.; Marshall, W. *Proc. Phys. Soc.* **1966**, *87*, 3–34.

amide anions which presumably exhibit an increased overlap with the metal d-orbitals. From our studies of $[\eta^4\text{-MAC}^*]^{4-}$ and related amido-*N* containing ligands with cobalt,[22,40] nickel,[41] and copper,[42] it can be deduced that a key bonding feature is that one of the metal d-orbitals is substantially destabilized as an antibonding orbital such that the electrons traditionally counted as the metal d-electrons become distributed among the four remaining d-orbitals. For the iron compounds described here, all the splittings among these four orbitals are sufficiently small that the $S = 2$ for iron(IV) and $S = {}^3/_2$ for iron(III) states are observed.

During the course of this study, Mössbauer and EPR spectroscopies and elemental analysis determinations were used to assess the purity of the iron compounds produced and thus to guide the search for spectroscopically suitable samples of the different materials.[43] According to the standards provided by application of these techniques, our complexes have a spectral and chemical purity of greater than 95%. Because of the unusual spin states found and the stabilities and high purities attained, we have initiated near-infrared optical and resonance Raman studies to further delineate the electronic structure of the novel complexes studied here. Moreover, since polycrystalline samples of both $[Fe^{III}Cl(\eta^4\text{-MAC}^*)]^{2-}$ and $[Fe^{IV}Cl(\eta^4\text{-MAC}^*)]^-$ yield well-resolved EPR spectra, single-crystal EPR studies will allow us to relate the ZFS-, A-, and EFG-tensors to the molecular coordinates of the complexes.

Acknowledgment. This work was supported by National Institute of Health Grants GM22701 (E.M.) and GM44867 (T.J.C.) and National Science Foundation Grant CHE-9019804 (T.J.C.). M.P.H. acknowledges an NIH Postdoctoral Fellowship (GM12996). K.L.K. acknowledges an AAUW American Fellowship.

Supplementary Material Available: Tables of data collection information, atom coordinates, Gaussian amplitudes, and bond lengths and angles (5 pages); a listing of structure factor amplitudes (10 pages). Ordering information is given on any current masthead page.

(40) Collins, T. J.; Powell, R. D.; Slebodnick, C.; Uffelman, E. S. *J. Am. Chem. Soc.* **1990**, *112*, 899–901.

(41) Collins, T. J.; Nichols, T. R.; Uffelman, E. S. *J. Am. Chem. Soc.* **1991**, *113*, 4708–4709.

(42) Collins, T. J.; Uffelman, E. S.; Woomer, C. G. Unpublished results.

(43) Throughout this study, we have found it necessary to work with several different salts of the $[Fe^{IV}Cl(\eta^4\text{-MAC}^*)]^-$ species in order to achieve the necessary purity for detailed spectroscopic studies. Several of the salts give excellent spectroscopic signatures but suffer from challenging purification problems. The salt, $[Et_4N][Fe^{IV}Cl(\eta^4\text{-MAC}^*)]$, has solubility properties similar to those of $[Et_4N][Cl]$ and $[Et_4N][ClO_4]$. The iron complex tends to crystallize as a mixture with these cation sources, making purification and iron quantitation difficult. For all the cations utilized here, the crystallization process must also compete with the slow conversion of iron(IV) to iron(III). For cations such as $[Bu_4N]^+$, this conversion rate could not be satisfactorily overcome to give large amounts of the pure iron(IV)-containing solid. The $[Ph_4P][Fe^{IV}Cl(\eta^4\text{-MAC}^*)]$ salt has proven easiest to handle and provides crystals that can be grown rapidly and reproducibly in large quantities and separated easily from iron(III) species to provide superior material for spectroscopy. However, this salt orders magnetically below ca. 9 K, limiting its use for determining spin Hamiltonian parameters.